PAPER

Check for updates

High spatial resolution WRF-Chem modeling in Quito, Ecuador†

Gabriela Mancheno[ab] and Héctor Jorquera [ID] *[ab]

The WRF-Chem model was applied for gas and aerosol chemistry in Quito, Ecuador, at a high horizontal resolution of 2 km. WRF-Chem was chosen due to its full coupling of meteorological and chemical processes, which is particularly suitable for complex topography and urban-scale simulations. Emission inventories were taken from EDGAR for the outer domains (32 and 8 km horizontal resolution), and local emission estimates were used for the innermost domain (2 km resolution) as initial estimates. The base year of simulation was 2018, and two months were chosen: April and December. WRF-Chem results were tested at five air quality stations across the Quito metropolitan area. To reduce bias between modeled and observed concentrations, Quito 2011 baseline emissions for CO, NO_x, SO_2, and $PM_{2.5}$ were adjusted by factors of 1.5, 0.75, 0.30 and 3.0 approximately, resulting in annual emission estimates of 300, 27, 1.5 and 7.5 kilotonnes per year (kton per year) for CO, NO_x (expressed as NO_2 equivalent), SO_2 and $PM_{2.5}$, respectively. The model run with these adjusted emissions showed good performance for CO, NO_x, SO_2, and O_3 ($r \sim 0.4$–0.8), but performance was lower for $PM_{2.5}$ ($r \sim 0.4$–0.5), particularly in the afternoon. This is ascribed mainly to an underestimation of secondary organic aerosol formation. The impact of biogenic VOC emissions on ozone and $PM_{2.5}$ is positive but small (+3–8%), and the inclusion of aerosol radiative feedback is minor ($\sim -0.5\%$), because of the relatively small ambient $PM_{2.5}$ concentrations in Quito.

Environmental significance

Urban atmospheric emission inventories are needed for developing urban air quality policies. However, these inventories include uncertainties coming mainly from the lack of emission factors tailored to the local context, which is the case in developing countries. The implementation of a state-of-the-science air quality model is an objective tool for improving these emission inventories. The application of the WRF-Chem model in the city of Quito, Ecuador, has led to a substantial improvement in available local emissions estimates. These updated emissions estimates would help researchers involved in air quality modelling tasks, such as urban air quality regulation or regional-scale air quality forecasts.

1 Introduction

In the Ecuadorian state, air pollution is one of its main environmental issues. Intense vehicular traffic and unplanned urban development are the major contributors to emissions of primary air pollutants.[1] However, they are not the only emission sources at play: the impacts of oil extraction and associated flaring activities in the Amazon region and the combustion of natural gas from deposits in the same area, non-metallic mining, the operation of thermoelectric plants for energy generation, and aerial fumigation in banana plantations on the Ecuadorian coast are other examples of problems associated with air pollution in Ecuador.[2]

Urban air quality management is an imperative facet of contemporary environmental stewardship, particularly in rapidly growing cities where the coexistence of industrial activities, vehicular emissions, and natural geographical constraints intensifies negative impacts on air quality and public health.[1,3] Quito, located in a narrow Andean valley at an elevation of 2850 meters, with steep surrounding terrain and limited horizontal air circulation, presents a challenging case for studying urban air quality dynamics.[4–6]

Within this context, our study focuses on the burgeoning metropolis of Quito, the capital city of Ecuador, situated within the Andean landscape. This introduction serves to delineate the scope and objectives of our research while contextualizing it within the broader discourse on urban air quality management.

The current state of the art in air quality simulation, especially for Ecuador and tropical countries with similar geographies such as Peru, Brazil, and Colombia (among others), has

[a]Departamento de Ingeniería Química y Bioprocesos, Pontificia Universidad Católica de Chile, Avda. Vicuña Mackenna 4860, Santiago 7820436, Chile. E-mail: jorquera@uc.cl

[b]Center for Sustainable Urban Development (CEDEUS), Los Navegantes 1963, Providencia, Santiago 7520246, Chile

been based on Eulerian chemical transport models, which constitute the central element for air pollution forecasting systems.[7–13] In Ecuador, only a few studies have applied or evaluated meteorological models using local data. Valencia *et al.*[5] modeled urban background pollution in Quito using a coarse resolution and limited observational validation. Moscoso-Vanegas *et al.*[14] modeled air quality in Cuenca, but their study also lacked detailed model evaluation. Parra[15–17] analyzed WRF and WRF-Chem performance for specific meteorological and chemical variables in the Andean region but did not conduct comprehensive urban modeling. Cazorla and Tamayo[18] described atmospheric measurements in Quito without applying or validating numerical models. These examples underscore the lack of systematic model evaluation efforts in Ecuador. Additionally, the evaluation of data in the vertical direction is almost nonexistent in tropical areas such as Ecuador[17] due to the scarcity of radiosonde data in the country. Despite its ecological significance and burgeoning population, Quito remains relatively understudied in the domain of air quality research, prompting the need for localized modeling efforts tailored to its specific context.[19]

Given the complex topography, meteorological variability, and spatial heterogeneity of emission sources in Quito, a three-dimensional Eulerian modeling framework is required. WRF-Chem was selected because it enables full online coupling of meteorological and chemical processes, which is critical for capturing feedback between local meteorology and pollutant dynamics, particularly in tropical mountainous regions. Compared to decoupled, off-line Eulerian or Lagrangean models, WRF-Chem provides enhanced realism and spatial resolution for urban-scale applications, precisely because of its fully coupled treatment of chemistry and meteorology.[20–22]

While mobile sources are recognized as the primary contributors to air pollution in Quito, other important sources were also considered. These include thermoelectric power plants, industrial emissions, the use of liquefied petroleum gas (LPG) in residential and commercial sectors, solvent use, and emissions from waste and area sources.[23] These categories are fully detailed in Section 2.2 and Table 2.

Moreover, ozone levels in Quito present a persistent issue, with exceedances of the regulatory 8-hour standard (100 μg m^{-3}) documented across several years. Details and supporting statistics are provided in Section 2.1 and Fig. 3. The implications of this problem and further details will be discussed in the monitoring section below. The primary objective of our study is twofold: first, to model the gas and aerosol chemistry within Quito's atmospheric domain and, second, to improve emission inventories for the city through advanced air quality modeling techniques. By using the WRF-Chem model, we seek to understand Quito's atmospheric composition and pollutant distribution, marking one of the first applications of such advanced modeling techniques in this region.

To achieve this objective, we combine empirical data, advanced chemical transport models, and high-resolution emission inventories.

2 Methods

2.1 Study area and monitoring stations

Quito is located on the eastern slopes of the Pichincha volcano in the western Andes, at an elevation of 2850 meters above sea level.[24] Positioned at the equator, it receives high solar radiation.[25] The city covers 372 km^2 (ref. 26) and had a population of 2 239 191 as per the 2010 census.[27] This population, along with the area coverage, includes both urban and rural areas within the Metropolitan District of Quito (DMQ), which is included in the innermost domain of the study (Fig. 1c). Quito's urban sprawl has led to significant urban heterogeneity.[28] Its mountainous terrain influences its layout, resulting in varied elevations and building heights.[4] Expansion into valleys and plains has increased population density in specific areas, affecting local weather and air quality.[24,28]

The city's climate, classified as 'tropical mountain' or 'Andean temperate' by INAMHI, features moderate temperatures with daily fluctuations, ranging from 10 °C to 20 °C.[29] Influences from the Humboldt Current and easterly trade winds create climatic variability.[30] Quito has a wet season from October to May and a dry season from June to September, with peak rainfall from March to May.[29,31]

In the city of Quito, the Metropolitan Atmospheric Monitoring Network (REMMAQ, for Red Metropolitana de Monitoreo Atmosférico de Quito) began its operation in mid-2003, and since January 2004, it has been providing air quality information. It primarily consists of an Automatic Monitoring Network (RAUTO, for Red Automática), composed of nine fixed stations, which are in each of the zonal administrations of the Metropolitan District of Quito (DMQ). These stations operate continuously 24 hours a day throughout the year, generating 10-min averaged concentrations for pollutants such as particulate matter (PM$_{2.5}$ and PM$_{10}$), carbon monoxide (CO), sulfur dioxide (SO$_2$), nitrogen oxides (NO$_x$), and ozone (O$_3$).[6]

Fig. 2 shows the monthly average concentrations of key air pollutants in Quito from 2004 to 2018, obtained from the REMMAQ. The values represent the average across all monitoring stations, providing an overview of air quality for the entire city. Carbon monoxide (CO) shows a significant decrease since 2004, stabilizing at low levels after 2008. Nitrogen dioxide (NO$_2$) concentrations exhibit significant variations with higher levels observed during the rainy season, particularly during peak traffic hours. This pattern has been associated with increased vehicular emissions and meteorological conditions that limit vertical dispersion of pollutants in Quito.[32]

The trends in air pollutant concentrations observed in Fig. 2 are influenced by several local factors, including topography, meteorology, vehicular and industrial emissions, regulatory policies, and episodic pollution events.[9,22,23,30,33] Quito is in a narrow high-altitude Andean valley approximately 2850 meters above sea level, which limits pollutant dispersion due to the surrounding steep terrain.[30] The city's complex mountain-valley wind system contributes to stagnation events, particularly during nighttime and early morning thermal inversions, which are common in the region and trap pollutants close to the
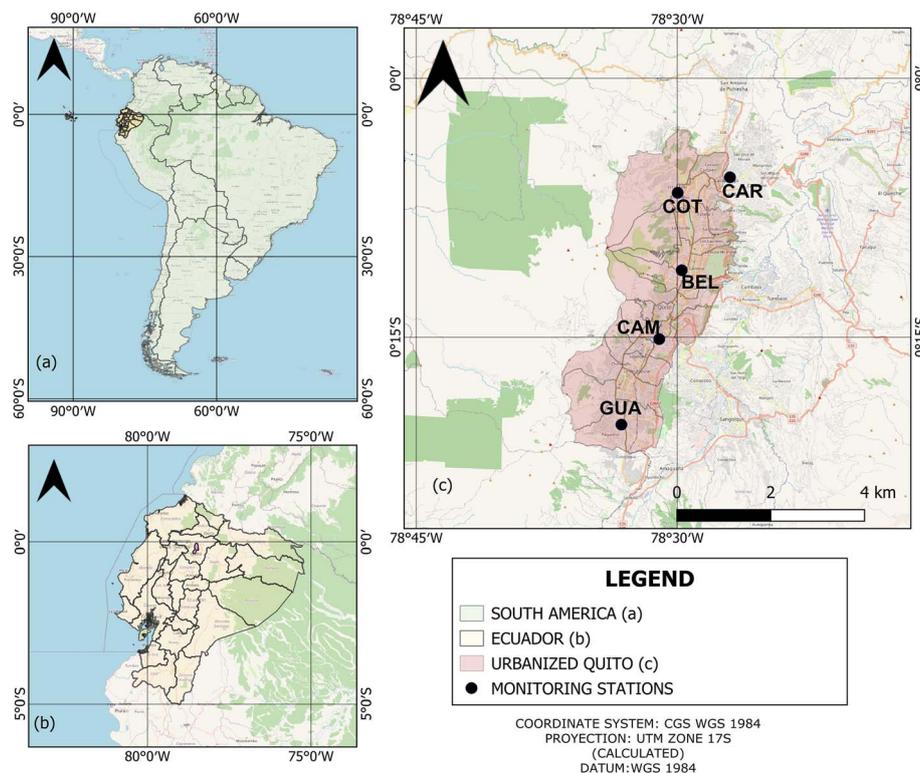
Fig. 1 Geographic location of the study area. (a) South America, highlighting Ecuador; (b) Ecuador, showing the location of Quito; and (c) the urbanized area of Quito, with the positions of the air quality monitoring stations (BEL, CAR, COT, CAM, and GUA). The basemap corresponds to OpenStreetMap imagery.

surface.[22] These conditions are particularly relevant for pollutants such as CO and NO_2, which exhibit higher concentrations during these hours.

Vehicular emissions represent the primary source of CO and NO_2 in Quito. The significant decrease in CO concentrations after 2004, followed by stabilization at lower levels post-2008, is consistent with fuel quality improvements and emission control policies.[34] Additionally, the implementation of the "Pico y Placa" vehicle restriction policy in 2010 likely contributed to reducing traffic-related emissions, although its long-term impact on air quality remains debated.[35,36] The variability in NO_2 concentrations, which lacks a clear long-term decreasing trend, may be linked to the increasing use of diesel-powered vehicles, which emit higher levels of NO_x despite fleet renewal efforts.[37] Regarding SO_2, high concentrations persisted until 2009, likely due to the use of high-sulfur fuels in industrial and vehicular sources.[23,38] The decline in SO_2 levels after 2009 coincides with the implementation of stricter fuel sulfur content regulations, which led to a shift toward low-sulfur fuels and reduced industrial emissions.[6] However, fluctuations in SO_2 concentrations may also be attributed to episodic volcanic activity, particularly from Cotopaxi (eruptions in 2015–2016) and Sangay (frequent eruptions since 2019), both of which have been shown to impact air quality in Quito.[33] These eruptions released significant quantities of SO_2 and particulate matter, with plumes occasionally reaching Quito depending on prevailing wind conditions. Finally, urban expansion and land-use

changes have influenced pollutant distribution by modifying traffic flow, increasing congestion, and altering emission source locations. As Quito continues to grow, the spatial redistribution of pollution sources may contribute to variations in pollutant concentrations across monitoring stations.[22]

In addition to mobile sources, other contributors to air pollution in Quito include emissions from thermoelectric power plants, industrial activities, residential and commercial combustion of LPG, solvent use, and biomass burning from both structural and forest fires.[23] These sources are reflected in the emissions inventory described in Section 2.2.

The interactions between O_3, NO_2, and SO_2 are influenced by photochemical reactions that depend on the availability of solar radiation and atmospheric oxidants. O_3 formation, for instance, consumes NO and influences NO_2 concentrations through photostationary equilibrium.[28,29] Similarly, precipitation plays a key role in the wet deposition and washout of particulate matter, particularly $PM_{2.5}$.[30] These dynamic processes are captured in WRF-Chem through its fully coupled meteorological and chemical mechanisms, allowing the model to account for seasonal variability in radiation, temperature, and rainfall, and their effects on pollutant formation and removal.

Ozone (O_3) shows variable concentrations with clear seasonal peaks, frequently exceeding 40 $\mu g\ m^{-3}$. O_3 concentrations exceeded the 100 $\mu g\ m^{-3}$ threshold in multiple years and across several stations during the 2004–2018 period, particularly at Carapungo and El Camal, indicating a recurring
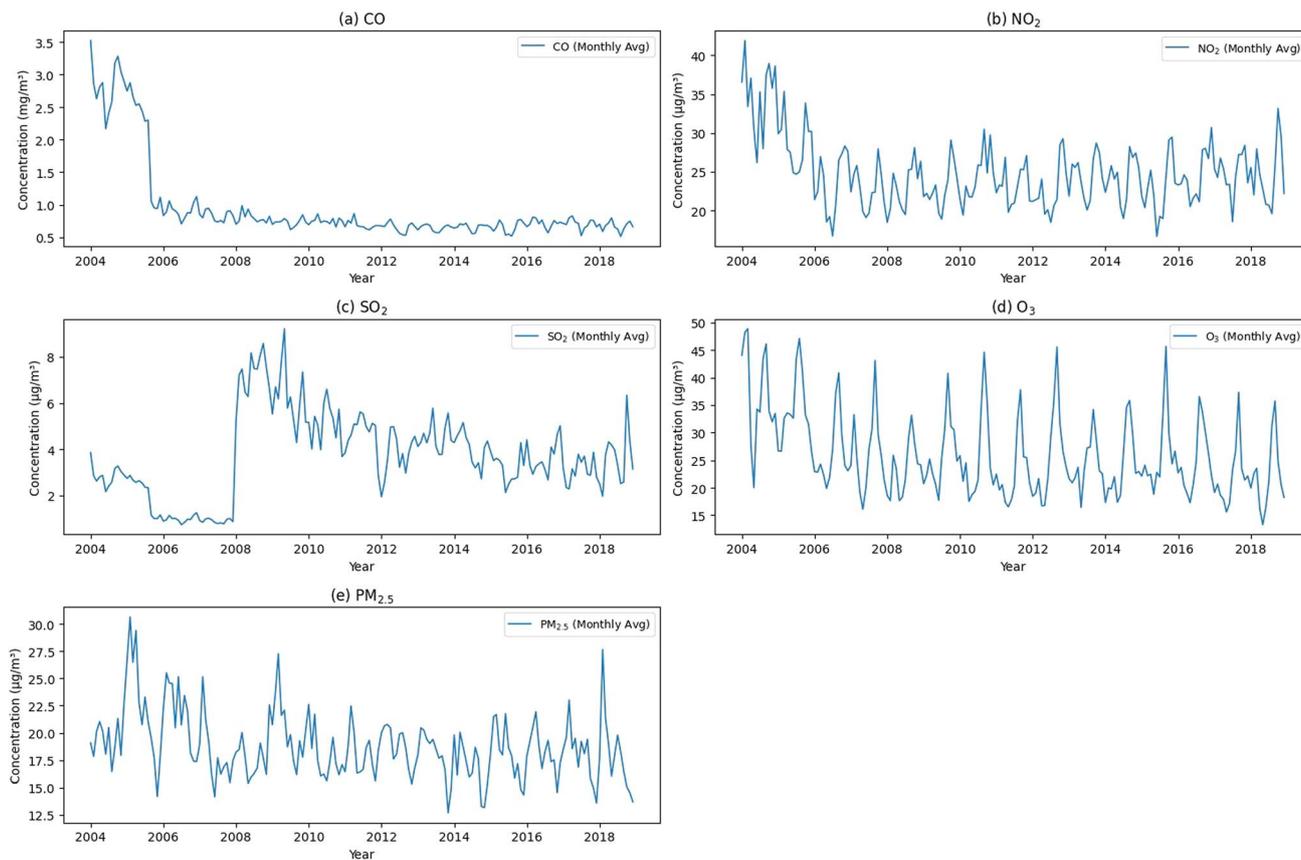
Fig. 2 Monthly average concentrations of key air pollutants in Quito from 2004 to 2018: (a) CO, (b) NO_2, (c) SO_2, (d) O_3, and (e) $PM_{2.5}$. Values represent the average across all monitoring stations of the Metropolitan Atmospheric Monitoring Network (REMMAQ), operated by the Secretaría de Ambiente of the Municipality of Quito. The authors do not own the monitoring network. The data are publicly available through the official website: https://ambiente.quito.gob.ec/.

air quality concern. According to the Ecuadorian regulation, as stated by the National Institute of Meteorology and Hydrology (INAMHI), the limit for ozone is set at 100 μg m^{-3} over an 8-hour average period.[39,40] Fine particulate matter ($PM_{2.5}$) presents significant fluctuations in concentrations, with several peaks over the years, showing a general downward trend but with notable seasonal variability.

Fig. 3 illustrates the trend in short-term ozone (O_3) concentrations over the years 2014 to 2018. The values presented represent the average across all monitoring stations in the city. This trend results from the combined influence of meteorological conditions (*e.g.*, high solar radiation, low wind speeds, and thermal inversions), emission sources (particularly vehicular traffic), and photochemical processes that regulate ozone formation and variability.[22,39] The data exhibit significant fluctuations with evident seasonal peaks, particularly during April and September, which coincide with periods of enhanced photochemical activity. These peaks are accompanied by frequent exceedances of the 100 μg m^{-3} limit for the 8-hour moving average ozone concentration established by Ecuadorian regulations.[29] Persistent exceedances—defined as multiple instances over several consecutive years—are clearly observable during this period. This pattern corroborates the findings of

Cazorla[39] and Alvarez-Mendoza *et al.*,[40] who reported chronic exceedances of ozone limits in Quito, underscoring the need for sustained monitoring and mitigation strategies. Furthermore, there is no observable decline in the frequency of these events between 2008 and 2018 (Fig. 3).

The names, geographic locations, and altitudes of the stations included in Table 1 were obtained from the Secretaría de Ambiente del Municipio de Quito (https://ambiente.quito.gob.ec/). Although the website provides general station metadata, the air quality and meteorological data used in this study were obtained through a formal data request. Table 1 includes the parameters measured at each station, their sampling frequency, and the year range covered in the analysis.

2.2 Annual emissions and their spatiotemporal distribution for Quito

The 2011 emissions inventory for the Metropolitan District of Quito (DMQ) was developed using previous inventories from 2003, 2005, 2007, and 2009,[41–44] and it is the starting point to build up the emission inventory for the innermost modeling domain (see Section 2.4 below) in the present work. The analysis area covers a square surface of 110 km per side, equivalent to 1°
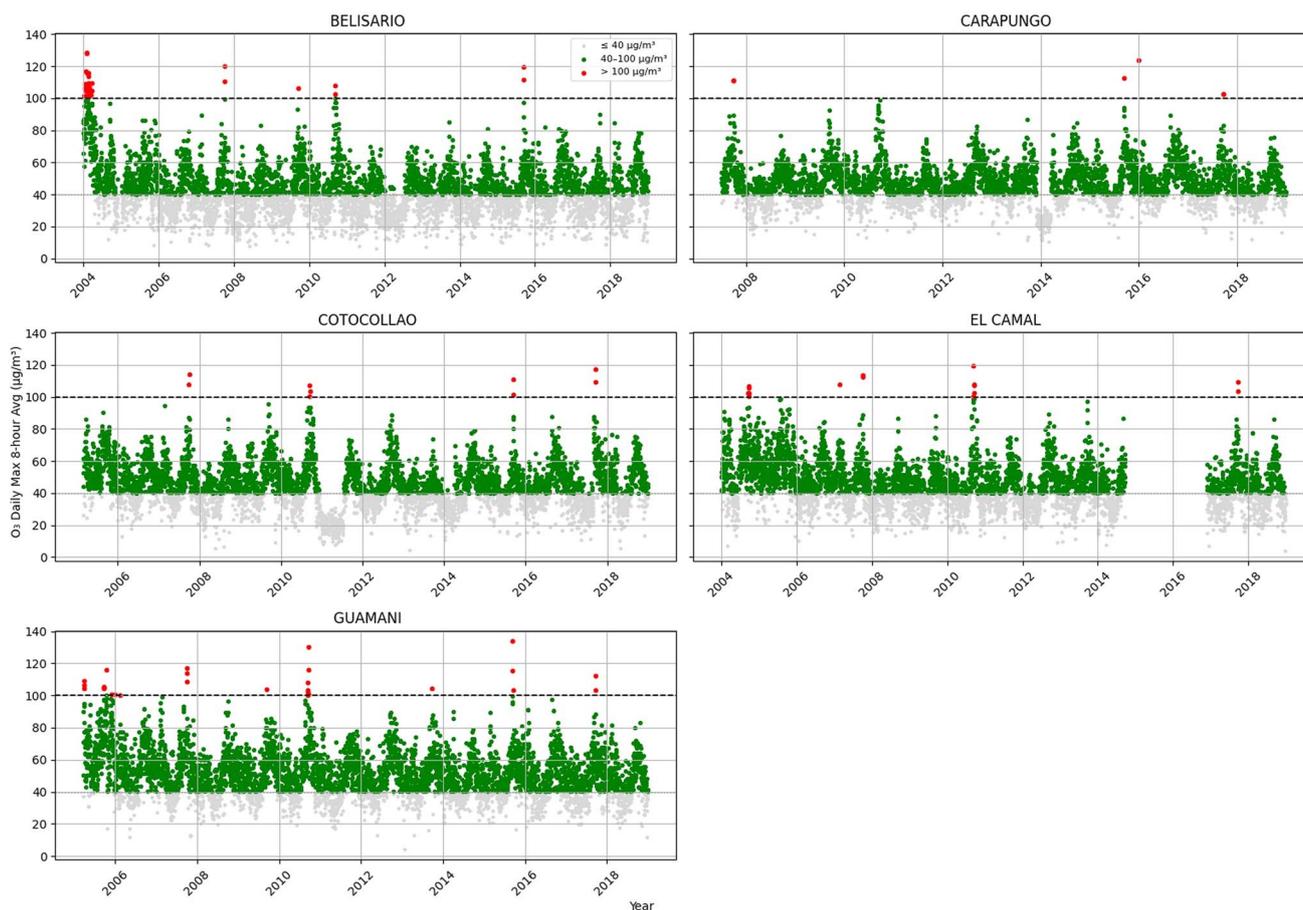
Fig. 3 Daily maximum 8-hour average ozone (O_3) concentrations from 2004 to 2018 at five monitoring stations in Quito: BELISARIO, CARAPUNGO, COTOCOLLAO, EL CAMAL, and GUAMANÍ. Red markers represent exceedances above the Ecuadorian regulatory standard[29] of 100 µg m^{-3} for 8-hour average O_3. Concentrations between 40 and 100 µg m^{-3} are shown in green to indicate periods of moderate exposure risk. The 40 µg m^{-3} threshold is commonly used in public health advisories and early warnings. These categories reflect both national air quality standards and WHO-based risk classifications. Data were provided by the Secretaría de Ambiente del Municipio de Quito and are accessible at https://ambiente.quito.gob.ec/.

Table 1 Monitoring stations for Quito.[a,b]

Code	Station	Longitude	Latitude	Altitude (m asl)	Measured parameters	Frequency	Data coverage
BEL	Belisario	−78.495677	−0.1851697	2835	O_3, NO_2, SO_2, CO, $PM_{2.5}$, temperature, wind, RH, pressure	10 min	2004–2018
CAR	Carapungo	−78.449413	−0.09548	2660	O_3, NO_2, SO_2, CO, $PM_{2.5}$, PM_{10} temperature, wind, RH, pressure	10 min	2004–2018
COT	Cotocollao	−78.49954	−0.11051	2795	O_3, NO_2, SO_2, CO, $PM_{2.5}$, temperature, wind, RH, pressure	10 min	2004–2018
CAM	El Camal	−78.517214	−0.2518482	2840	O_3, NO_2, SO_2, CO, $PM_{2.5}$, temperature, wind, RH, pressure	10 min	2004–2018
GUA	Guamaní	−78.553478	−0.3342668	3066	O_3, NO_2, SO_2, CO, $PM_{2.5}$, temperature, wind, RH, pressure	10 min	2004–2018

[a] Source: Secretaría de Ambiente del Municipio de Quito (https://ambiente.quito.gob.ec/). [b] Although all stations in the Metropolitan Air Quality Monitoring Network (REMMAQ) measure fine particulate matter ($PM_{2.5}$), gaseous pollutants (CO, NO_2, SO_2, and O_3), and meteorological variables, only the Carapungo station is equipped with sensors for coarse particulate matter (PM_{10}). This distinction is based on validated data sources and historical reports of Quito's air quality monitoring efforts. The meteorological variables include temperature, wind (both speed and direction), relative humidity (RH), and atmospheric pressure. Measurements are automatically recorded every 10 minutes; however, data are not consistently available across all months and years due to periodic equipment maintenance, calibration, or operational issues. Although the table shows a general data range from 2004 to 2018, users must verify completeness for specific periods of interest.

of latitude/longitude, encompassing 12 323 km^2 and including the entire Metropolitan District of Quito. The inventory includes pollutants such as nitrogen oxides (NO$_x$), non-methane volatile organic compounds (NMVOCs), particulate matter less than 10 and 2.5 microns (PM$_{10}$ and PM$_{2.5}$, respectively), ammonia (NH$_3$), carbon monoxide (CO), and sulfur dioxide (SO$_2$).[23]

Given the absence of locally derived emission factors, most values were sourced from peer-reviewed studies and emission inventories conducted in Mexico and the United States, where urban conditions and transportation emissions are comparable to those in Quito.[5,23] Additionally, to enhance the spatial and temporal accuracy of emissions, refinements were applied in the innermost modeling domain. These included the use of traffic intensity measurements and fuel consumption data, local emission factors for gasoline vehicles, and monthly and hourly emission profiles tailored to the Quito's urban context.[45–48]

Emission sources are categorized into three main groups: mobile, stationary, and area sources (Table 2). Mobile sources include emissions from on-road vehicles (light-duty gasoline and diesel vehicles, public buses, taxis, and motorcycles) and aircraft operations at the Mariscal Sucre Airport. Stationary sources encompass emissions from thermoelectric power plants and industrial facilities engaged in manufacturing, food processing, and fuel combustion. Area sources comprise biogenic emissions (from vegetation and soil), residential and commercial use of liquefied petroleum gas (LPG) and solvents, residential ammonia (NH$_3$) emissions from domestic waste and cleaning products, emissions from gas stations and fuel depots, dust from paved and unpaved roads, wind erosion, quarrying activities, forest fires, and structural fires, which refer to fires occurring in buildings and other human-made structures (*e.g.*, residential or industrial facilities). Unlike previous inventories, the 2011 inventory did not evaluate emissions from barbecues and brick kilns due to their relatively low contribution.[23]

The 2011 emissions inventory was selected for the 2018 simulations because it represents the most comprehensive and detailed dataset available for the region at the time of modeling. Although inventories for 2003, 2005, 2007, and 2009 exist, they were developed using generalized emission factors and national-level activity data, without adequate spatial disaggregation. No validated inventories were found for 2013 or 2015 that met the requirements for urban air quality modeling. More recent efforts, such as a traffic-based emission study[49] from 2012 or a 2015 carbon footprint inventory (Ecuadorian

Greenhouse Gas Inventory[50]), were limited in scope and focused on specific sectors or greenhouse gases. In contrast, the 2011 inventory incorporated locally collected data and was refined using high-resolution proxy variables such as road network density, population distribution, and sectoral fuel consumption to enhance the spatial allocation of emissions within the innermost domain. These features made it the most appropriate base for simulations conducted in this study. This limitation is acknowledged as a constraint in the present study and reflects the broader challenges of emissions data availability in developing countries. While more recent global inventories, such as EDGAR HTAPv3,[51] provide emissions data up to 2018, they lack the high spatial resolution required to accurately represent emissions at the urban scale in Quito. The use of a locally developed inventory allowed for a better representation of urban emission patterns, making it a more suitable choice for modeling air quality in the region.

A horizontal resolution of 2 km was selected as a trade-off between spatial accuracy and computational feasibility. WRF-Chem simulations with online chemistry, multiple nested domains, and multi-month runs are computationally intensive. Preliminary tests using a 1 km resolution did not yield significant improvements in model performance but led to a considerable increase in computational burden and data processing time, associated with reduced integration time steps to keep numerical stability. Similar resolutions have been effectively used in cities with complex terrain and data constraints.[8,9]

Regional background contributions (boundary conditions) were handled using a nesting strategy. Anthropogenic emissions from EDGAR were applied to the outer domains (32 km and 8 km), capturing regional-scale processes, while the 2 km innermost domain relied on a refined local inventory. Through dynamic boundary conditions, regional pollutants are transported into the urban domain, ensuring a realistic representation of regional contributions at finer scales.

2.3 The weather research and forecasting model (WRF)

The Weather Research and Forecasting Model with Chemistry (WRF-Chem), a numerical model, simulates the main physical and chemical processes at urban, regional (basin), and synoptic (country) scales. To model gas and aerosol chemistry and estimate emission inventories in Quito, the WRF-Chem (Version 4.4)[52,53] model was employed with three nested spatial domains at 32, 8, and 2 km horizontal resolutions. Anthropogenic emission inventories from EDGAR were processed using

Table 2 Annual emissions in DMQ, 2011 (tons per year)^a

Sources	CO	SO$_2$	NO$_x$	PM$_{10}$	PM$_{2.5}$	NMVOC	NH$_3$
Mobile sources	77 978	1166	17 344	1095	832	11 935	396
Stationary sources	686	3582	7037	372	226	5614	88
Area sources	462	5	680	1825	278	20 792	1442
Total	79 126	4753	25 060	3292	1337	38 341	1926

^{a} Source: Distrito Metropolitano de Quito, Secretaría de Ambiente, 2014. Informe Final Inventario de Emisiones de Contaminantes Criterio, DMQ 2011. Author: Juan Carlos Baca.

© 2025 The Author(s). Published by the Royal Society of Chemistry

Environ. Sci.: Adv., 2025, **4**, 1310–1332 | **1315**

HERMES-v3 software.[54] The innermost domain's inventory was spatially distributed based on industrial point sources' location, population density data from the Global Human Settlement Layer (https://human-settlement.emergency.copernicus.eu/), and vehicle counts at 110 measuring points across the city, accounting for industrial, residential, and road traffic sources, respectively.[3,55] Biogenic VOC emissions were estimated in real-time using the MEGAN model within the WRF-Chem framework, while the chosen chemical mechanism was CBMZ with MADE/SORGAM aerosols (mechanism 30 in WRF-Chem).[54,56]

In this study, we obtained the global meteorological data required to generate boundary and initial conditions for WRF from meteorological reanalysis accessible at the National Centers for Environmental Prediction (NCEP), FNL Operational Model Global Tropospheric Analyses featuring a spatial resolution of 0.25° updated every six hours.[57] These data were input to the WRF Preprocessing System (WPS) to generate IC and BC WRF input files.

While WRF-Chem was selected for this study due to its fully coupled treatment of meteorology and chemistry, other models are available for regional air quality modeling. Offline models such as CMAQ[58] or CHIMERE[59] simulate regional-scale transport using meteorological inputs from external models. However, they do not allow feedback between chemistry and meteorology, which can be important in dynamic regions such as the tropical Andes. This decoupling may lead to errors in predicting pollutant concentrations influenced by meteorology-sensitive processes such as ozone photochemistry or aerosol–radiation interactions.[58,59] Lagrangean models, although computationally efficient for simulating plume dispersion of tracer species or specific source tracking, are not well suited for simulating the complex spatial distribution of pollutants in topographically constrained cities such as Quito. Their limited ability to represent chemical transformations and background accumulation from multiple sources can result in an underestimation of secondary pollutant formation and urban-scale concentrations.[60] These considerations support the use of an online Eulerian model such as WRF-Chem to better capture the interplay between meteorology, emissions, and chemical transformations across scales.

The base year of simulation, 2018, includes April and December as focal months for testing emission inventories to account for seasonal variations. April represents one of the rainy peaks, capturing the cooler and wetter conditions, while December, despite being part of the rainy season, often experiences a small summer or a short period of sunny and warm weather. These months were selected to ensure the model accounts for the distinct climatic conditions affecting air quality throughout the year.[61] We tested several planetary boundary layer schemes, including Yonsei University (YSU), Mellor–Yamada–Janjic (MYJ), Mellor–Yamada–Nakashini–

Table 3 WRF Chem configuration and parameterization

Parameter & domains			Model configuration
max_dom			=3
e_we			=75, 105, 77
e_sn			=75, 105, 69
e_vert			=53, 53, 53
p_top_requested			=5000
num_metgrid_levels			=32
num_metgrid_soil_levels			=4
dx			=32 019.11, 8004.778, 2001.194
dy			=32 019.11, 8004.778, 2001.194
dzbot			=20
smooth_option			=0
use_surface			=.true
force_sfc_in_vinterp &physics and &chem			=1
Planetary boundary layer	YSU		Hong et al.[62]
	MYJ		Janjić[63]
	MYNN2		Nakanishi & Niino[64]
	BouLac		
Microphysics	WSM6		Hong, & Lim[65]
Radiation			
Longwave	RRTMG		Iacono et al.[66]
Shortwave	RRTMG		Iacono et al.[66]
Surface layer	MM5 similarity		Paulson;[67] Dyer & Hicks;[68] Webb;[69] Jiménez et al.[70]
Surface physics	Unified Noah Land Surface Model		Tewari et al.[71]
Urban surface physics	Building Environment Parameterization (BEP) scheme		Martilli et al.[72]
Cumulus	Grell 3D ensemble scheme		Grell & Dévényi[73]
Chemical mechanism	CBMZ chemical mechanism and MADE/SORGAM (Modal Aerosol Dynamics Model for Europe/Secondary Organic Aerosol Model) modal aerosol		Stockwell et al.,[74] Ackermann et al.,[75] and Schell et al.[76]

Niino 2.5 (MYNN2), and Bougeault–Lacarrere (BouLac) to assess their efficacy in capturing Quito's atmospheric dynamics.[18,56] Cumulus and aerosol radiative feedback are also integrated into our model configuration (Table 3).

2.3.1. Model configuration. The horizontal domain includes three nested unidirectional domains, centered at 2° 12′0.00″ S and 79°0′21.388″ W, with horizontal spacings of 32, 8, and 2 km, as depicted in Fig. 4. These three domains span 75, 105 and 77 cells in the E–W direction and 75, 105 and 69 cells in the N–S direction, respectively. This configuration provides enhanced spatial resolution, effectively capturing atmospheric phenomena at finer, local scales. The innermost domain, with a 2 km grid spacing, encompasses the urban area of Quito (Fig. 4).

The selection of spatial scales for emissions was designed to ensure consistency with the WRF-Chem model resolution and atmospheric processes. The horizontal allocation of emissions followed the model grid resolution, with EDGAR v4.3.2 emissions[77] processed at 32 km and 8 km resolutions for the outer domains, while a high-resolution local emissions inventory (2011) was applied at 2 km for the innermost domain to better capture urban-scale pollution sources. Compared to EDGAR v4.3.2, which provides emissions at a coarse global resolution (∼0.1°) and uses uniform default emission factors, the 2011 local inventory offers significantly higher spatial detail (2 km) and incorporates local data for key sectors such as traffic, fuel consumption, and industry. These differences are critical at the urban scale, where emission patterns vary strongly by zone, and fine-scale resolution is essential for capturing pollutant gradients in complex terrains such as Quito. This approach ensures that emissions reflect the scale of their dominant processes, with large-scale transport captured in coarser domains and localized emissions preserved at finer scales.

Vertically, emissions were distributed across multiple model levels based on WRF-Chem's vertical grid structure. Surface emissions, such as those from traffic and residential sources, were allocated to the lowest model levels (∼20 m AGL) to ensure realistic near-surface concentrations. Industrial emissions were
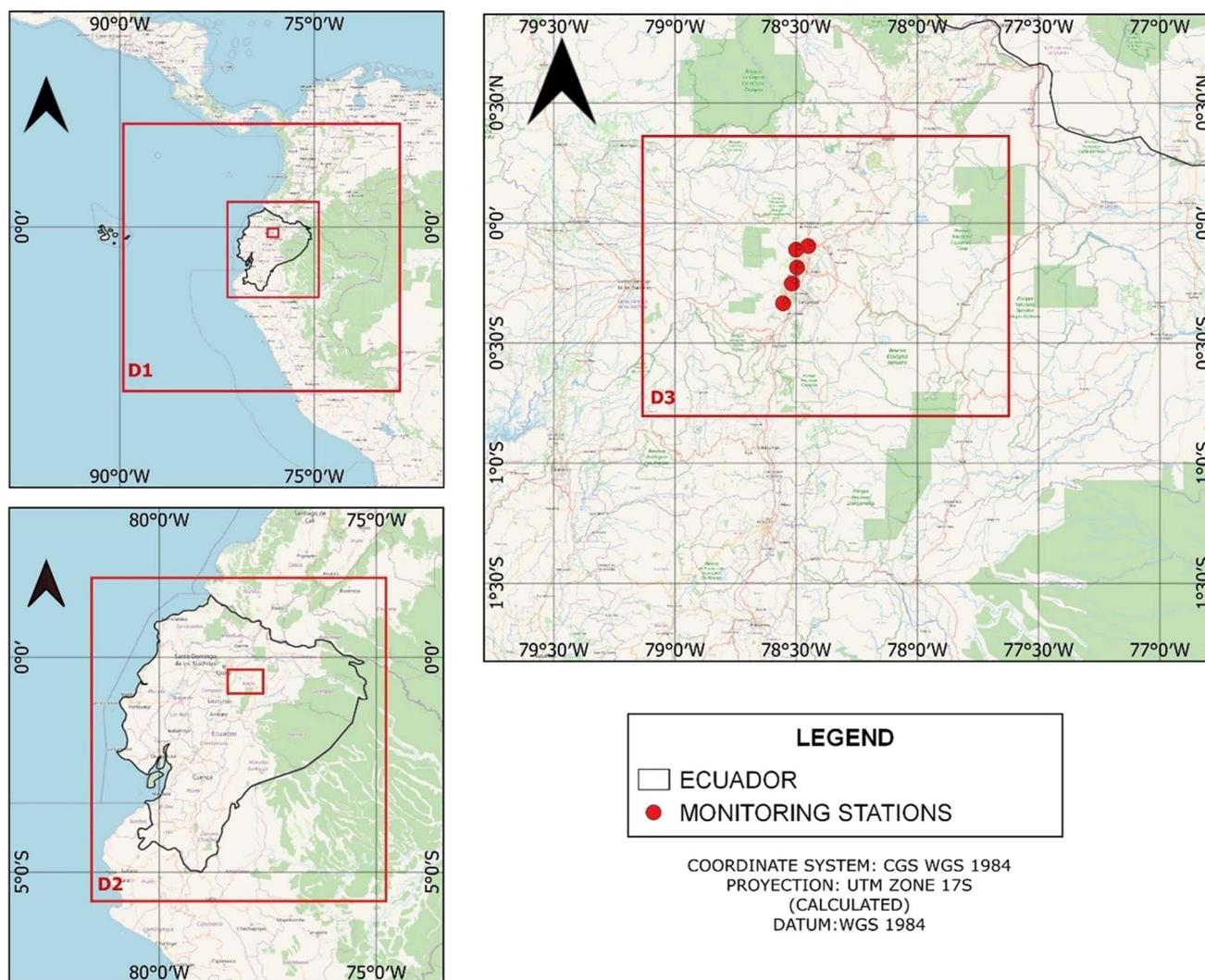

Fig. 4 Nested domains used in the WRF-Chem simulations: D1 (continental scale), D2 (regional scale), and D3 (local scale over Quito). Only the innermost domain (D3), which includes the monitoring stations used for model evaluation, was employed for retrospective simulations.

© 2025 The Author(s). Published by the Royal Society of Chemistry

Environ. Sci.: Adv., 2025, **4**, 1310–1332 | **1317**

treated in a simplified manner, as no specific stack height data (neither stack exit gas temperature and velocity) were available for Quito's industries. This study did not use radiosonde data for vertical validation due to the lack of available measurements in Ecuador. The vertical distribution of elevated (industrial and energy generation) emissions followed default profiles from HERMES v3, which is a standard approach under data-scarce conditions. This assumption was necessary due to the absence of more detailed source information, but it still allows for dispersion of industrial pollutants across the planetary boundary layer height. This method introduces limitations in representing elevated sources but remains a common practice in urban-scale modeling under data-scarce conditions. The profiles categorize emissions by source type and assign them to model levels in WRF-Chem's vertical grid, enabling the simulation of vertical pollutant dispersion in the planetary boundary layer.[21,54]

The horizontal distribution of emission sources in the WRF-Chem model was implemented using specific local datasets for each source type. Traffic emissions were spatially allocated based on georeferenced data from 110 vehicle counting stations in Quito, which allowed for the assignment of emissions to the model grid cells. This information was further complemented by population density data from the Global Human Settlements Layer (GHSL) to adjust emissions according to areas with higher vehicular activity. Then, the product of vehicle activity and population density was used as a proxy of traffic emissions. This approach effectively captured spatial variations in traffic emissions across the city. Industrial emissions and energy generation units were distributed based on the geographic locations of their facilities, ensuring accurate alignment of emission sources with the model grid.

For temporal allocation, diurnal and weekly traffic emission profiles were incorporated, derived from vehicle count data. These profiles reflect typical traffic patterns, such as peak hours during weekdays and reduced activity on weekends and holidays. These temporal variations were processed using HERMES-v3 to ensure that emissions realistically captured daily and weekly variability observed in the city. Additionally, MATLAB scripts were employed to process and allocate traffic emissions spatially and temporally within the urban domain, based on the above profiles. All codes and ancillary files are available in a public data repository (see Data availability statement below).

2.3.2. WRF model parameterization. The WRF model offers a versatile array of options for modeling physical processes, which can range from short-term to long-term predictions, thereby making it highly adaptable to specific case study requirements.[52,78,79] These options encompass parameterizations for the planetary boundary layer (PBL), land and urban surfaces, cloud microphysics, and radiation, all of which are critical for air quality research.[80–82]

In this study, we assessed the sensitivity of air quality simulations to different PBL parameterizations by examining five schemes: Yonsei University (YSU), Mellor–Yamada–Janjic (MYJ), Mellor–Yamada–Nakanishi and Niino Level 2.5 (MYNN2), and Bougeault–Lacarrere (BouLac). The microphysics scheme used was WSM6, and radiation processes were carried out using the RRTMG scheme (long and short wave). Surface physics was represented using the Unified Noah Land Surface Model, while cumulus processes were simulated with the Grell 3D ensemble scheme.

To improve the representation of meteorological conditions at the urban scale, the Building Environment Parameterization (BEP) scheme[72] was utilized for urban surface physics, combined with the YSU, MYJ and BouLac PBL schemes. The chemical mechanism chosen was CBMZ and the aerosols were modeled with the MADE/SORGAM aerosol mechanism (see Table 3 for details).

The selection of physical schemes for this study was based on their proven suitability for high-resolution, urban-scale simulations in complex terrain. The planetary boundary layer (PBL) schemes selected—YSU, MYJ, MYNN2, and BouLac—have been previously tested in Ecuador and the Andes region, showing differential capacity in reproducing diurnal variation and pollutant dispersion in high-altitude environments.[16,17] The RRTMG radiation scheme and WSM6 microphysics were chosen due to their established performance in tropical regions and their compatibility with CBMZ chemistry. The Unified Noah land surface model and BEP urban scheme were included to better resolve surface-atmosphere interactions in Quito's heterogeneous urban landscape.

The WRF physical configuration used in this study has been evaluated by Mancheno et al.,[83] where multiple parameterization schemes—including those adopted here—were tested over Quito. That work assessed WRF's ability to reproduce key meteorological variables such as 2-meter temperature, wind speed, relative humidity, and planetary boundary layer height (PBLH), and found that YSU and MYNN2 schemes, in combination with RRTMG radiation and BEP urban surface physics, provided the best agreement with observations. These results validated the use of this configuration as a reliable meteorological foundation for the air quality simulations presented in this study.

Although the sensitivity analysis was conducted on meteorological configurations, the results also reflect how model physics affects the transport and dilution of emissions from various sources. For example, differences in boundary layer height, turbulence, and vertical mixing directly impact the modeled concentrations of near-surface pollutants, particularly those emitted from traffic or industrial areas.

2.4 Evaluation of air quality model performance

The WRF model's performance was assessed using data from five monitoring stations (Table 1), which were selected based on their spatial distribution across Quito and the completeness of their data records. Only stations with at least 75% data availability—defined as having valid hourly measurements for at least 75% of the total hours during the study period—were included in the analysis. This threshold follows standard guidance for air quality model evaluation, ensuring robust temporal coverage and minimizing uncertainty due to missing data.[6,99]

A total of 8 WRF-Chem simulations were conducted, considering four PBL schemes for two months (April and December). Pollutant concentrations were analyzed at five monitoring stations for five different pollutants, applying correction factors to emissions. The final dataset includes 200 individual pollutant-station-month combinations. Out of the four simulations per month, three included BEP urban schemes, corresponding to the YSU, BouLac, and MYJ PBL schemes. The fourth simulation used the MYNN2 PBL scheme with sf_urban_physics = 0, meaning no urban canopy model was activated. Each simulation evaluated five key atmospheric pollutants: sulfur dioxide (SO_2), carbon monoxide (CO), nitrogen oxides (NO_x), ozone (O_3), and particulate matter with an aerodynamic diameter of 2.5 micrometers or less ($PM_{2.5}$).

Performance metrics such as the Neyman–Pearson correlation coefficient (r), mean bias (MB), normalized mean bias (NMB), normalized mean gross error (NMGE), root mean square error (RMSE) and agreement factor (FAC) were computed.[84] These metrics provided insights into the model's ability to accurately simulate pollutant concentrations and their spatial and temporal variations. Additionally, the impact of different emission inventory adjustments on model performance was analyzed using those metrics as guidance. Each metric was scored using an ordinal scale from 1 (worst) to 4 (best) based on relative performance across model configurations. For error-based metrics (MB, NMB, NMGE, and RMSE), lower values indicated better performance; for r and FAC2, higher values were preferred. The individual metric scores were then summed (with equal weight) to compute an overall performance score for each configuration, station, and month. This scoring approach integrates multiple dimensions of performance—bias, error magnitude, and correlation—into a single comparative framework without assuming interdependence among metrics. The use of additive, rank-based evaluations is consistent with previous practices in air quality modeling assessments.[85,86] The mathematical expressions of these metrics are not included here, as they follow standard definitions widely documented in the literature. Full scoring details and results are provided in ESI Table S1.† This selection of optimal configurations was conducted using simulations based on uncorrected emissions, ensuring that the identification of best-performing model settings was independent from the subsequent application of emission correction factors. Each pollutant was evaluated separately, recognizing that different chemical and transport processes influence model performance depending on species. Scores were computed per station and averaged to ensure spatial representativeness, without giving additional weight to any single site. This stepwise and pollutant-specific evaluation approach enhances robustness and aligns with established methodologies in model intercomparison studies.[85,87]

An initial evaluation revealed systematic underestimations for CO and $PM_{2.5}$ and overestimations for SO_2 and NO_x. It was assumed that the greater source of uncertainty in the above simulations came primarily from the initial emission inventory. Then, in a second set of simulations, correction factors were applied to improve agreement between modeled and observed concentrations. Finally, emissions in the innermost domain were scaled by factors of 1.5, 0.75, 0.30 and 3.0 for CO, NO_x, SO_2 and $PM_{2.5}$, resulting in annual emission estimates of 300, 27, 1.5 and 7.5 kilotonnes per year (kton per year) for CO, NO_x (expressed as NO_2 equivalent), SO_2 and $PM_{2.5}$, respectively. These adjustments were applied uniformly across the innermost domain, maintaining the temporal and spatial structure of the initial inventory. The same factors were used for April simulations, assuming consistent seasonal behavior within the wet season. In this context, the correction factors serve as a practical and justified approach to calibrate the system under data-scarce conditions and improve the reliability of modeled pollutant levels, consistent with methodologies applied in other urban-scale modeling studies.[22,88]

In the case of $PM_{2.5}$, we performed additional simulations that included regional biomass burning emissions in domains 1 and 2 and tested different vertical profiles for their injection height, using the FINN2.5 updated emission inventory.[89] The results showed that inclusion of these emissions produced small changes in the hourly average concentrations across monitoring stations in Quito (see Section 3.5 below). Thus, the remaining underestimations were attributed to the local inventory limitations; this justifies the use of adjustment factors only in domain 3.

3 Results and discussion

In this section, we present the modeling results and their analysis. All modeled scenarios are presented for each pollutant, with observed data represented in red. The results for December 2018 are presented below, and the corresponding results for April—wet season—are presented in the ESI.† The statistical results for December are shown in Tables S1 to S5,† and for April in Tables S6 to S10,† all of which are included in the ESI.†

3.1 CO

Fig. 5 displays all modeling results and observations for December, and the statistical results are presented in Table S1 in the ESI.† The observed CO levels exhibit a clear bimodal pattern with peaks during the early morning and late evening, corresponding to rush hour traffic. This pattern, consistent across all monitoring stations, confirms that vehicular emissions are the predominant source of CO in Quito, as reflected in the emissions inventory.

The MYNN2 model was selected for detailed discussion as it demonstrated the best overall performance across the different monitoring stations, based on the statistical indices (Table S1†). At the Belisario and El Camal stations, the MYNN2 model showed a strong alignment with observed data, effectively capturing the daily CO variations and peak concentrations. Despite some minor discrepancies, such as a slight underestimation at El Camal, the model's ability to track the general trend suggests that it accurately represents the primary emission processes influencing these areas.

The spatial configuration of the air quality monitoring network in Quito is concentrated in areas of high population density and vehicular activity, which inherently reinforces the
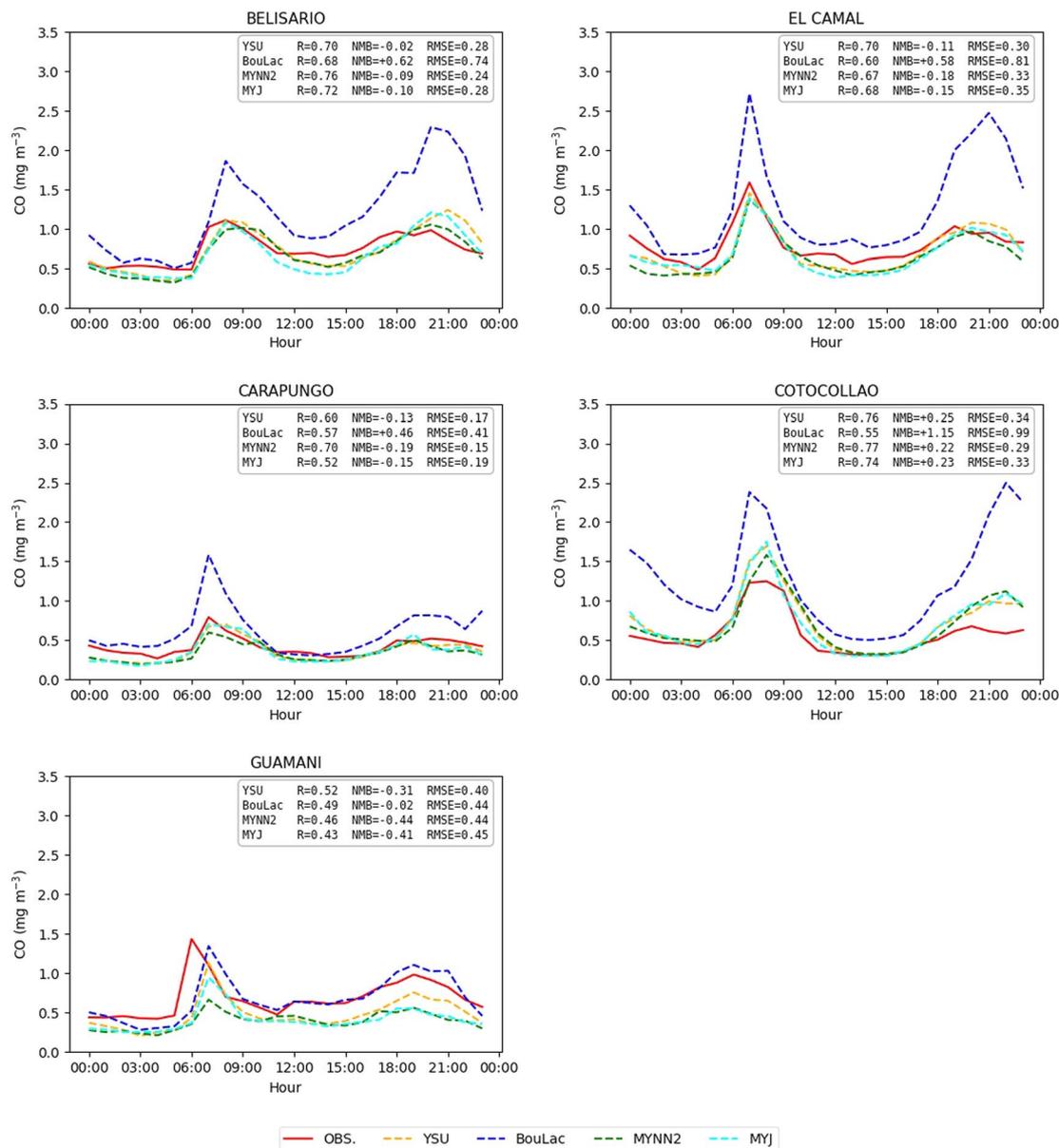
© 2025 The Author(s). Published by the Royal Society of Chemistry

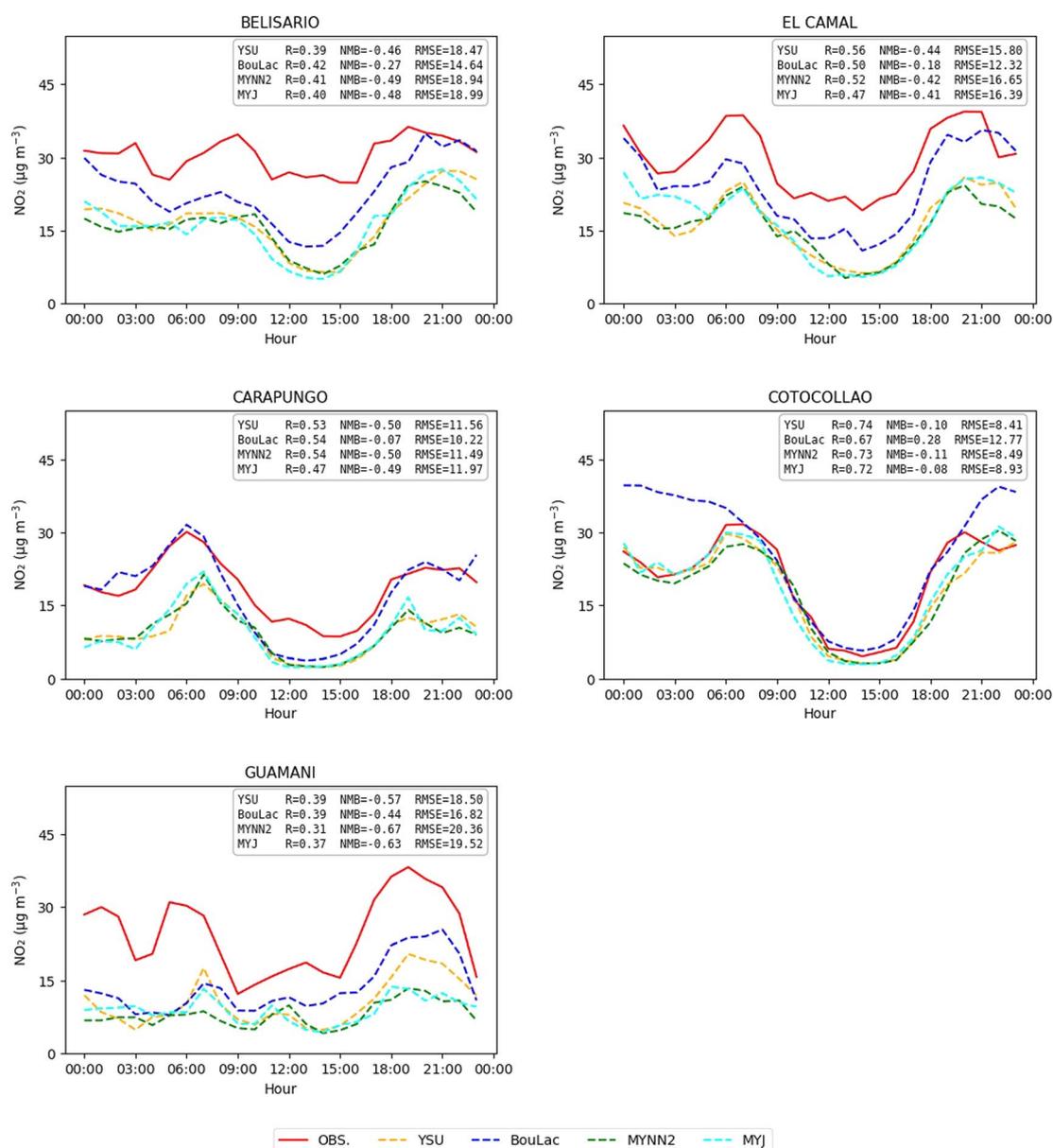*Environ. Sci.: Adv.*, 2025, **4**, 1310–1332 | **1319**

Fig. 5 Hourly average CO concentrations at selected monitoring stations in Quito during December. The figure compares observed data (red solid line) with model simulations using four planetary boundary layer (PBL) schemes: YSU, MYJ, MYNN2, and BouLac. The curves represent daily averages by hour and are used to assess each configuration's ability to reproduce the diurnal cycle of CO. Statistical performance indicators (MB, NMB, RMSE, and r) are shown in each panel for each model.

dominant role of mobile sources in shaping observed CO concentrations. According to the official 2011 emissions inventory published by the environmental secretariat of Quito,[23] mobile sources accounted for 98.5% of total CO emissions, with the remaining contributions distributed between industrial combustion and residential LPG use.

Although the inventory includes disaggregated activity data by vehicle category (*e.g.*, light-duty gasoline vehicles, diesel buses, and motorcycles), it does not incorporate technological classifications such as EURO standards or fleet age structure, as such information is not systematically collected in Ecuador.

The contribution of fixed sources, such as thermal power plants and industrial facilities, is relatively minor for CO. For instance, total annual emissions from the Guangopolo and Gualberto Hernández thermal plants summed only 302 tons, which is less than 0.4% of total CO emissions.[23] These findings support the conclusion that modeled and observed CO concentrations are primarily influenced by mobile sources, particularly in central Quito.

At the Carapungo and Cotocollao stations, the model continues to perform well, albeit with some differences in bias direction. At Carapungo, the model's performance is similar to that at El Camal, accurately following the observed CO

1320 | *Environ. Sci.: Adv.*, 2025, **4**, 1310–1332

© 2025 The Author(s). Published by the Royal Society of Chemistry

fluctuations with a tendency toward underestimation. Meanwhile, at Cotocollao, the model slightly overestimates CO levels but still captures the overall trend.

The most significant challenges arise at the Guamaní station, where the model struggles to replicate the observed CO levels, particularly during peak pollution periods. This underperformance could be attributed to unique local factors not fully captured by the emissions inventory or model configuration, such as specific microclimatic conditions or unaccounted-for sources.

In April, as shown in Fig. S2,† the MYNN2 model continues to provide the closest match to observed CO levels, particularly

during peak traffic hours. This consistency across two different months reinforces the model's robustness in simulating traffic-related CO emissions in Quito.

3.2 NO₂

Fig. 6 illustrates the model performance in simulating NO_2 concentrations, with the detailed statistical results provided in Table S2 of the ESI.†

Although the emission inventory used includes NO_x (NO + NO_2), the WRF-Chem model (CBMZ mechanism) simulates NO and NO_2 as separate species. This section focuses exclusively on NO_2 because it is the species measured at monitoring stations

Fig. 6 Hourly average NO_2 concentrations at selected monitoring stations in Quito during December. The figure compares observed data (red solid line) with model simulations using four planetary boundary layer (PBL) schemes: YSU, MYJ, MYNN2, and BouLac. The curves represent daily averages by hour and are used to assess each configuration's ability to reproduce the diurnal cycle of NO_2. Statistical performance indicators (MB, NMB, RMSE, and r) are shown in each panel for each model.

© 2025 The Author(s). Published by the Royal Society of Chemistry

Environ. Sci.: Adv., 2025, **4**, 1310–1332 | **1321**

in Quito. The model results shown correspond to NO_2 output from the chemical mechanism, not to total NO_x.

The BouLac model, which is discussed here because it presented the best statistical results among the models tested, generally captures the temporal patterns of NO_2 across the stations. However, as with most models, there is a tendency to slightly underestimate NO_2 levels, particularly at the Belisario and Guamaní stations. This suggests that while BouLac performs well overall, there may be specific local factors or emission sources that are more challenging to represent accurately.

Interestingly, at the Carapungo station, the BouLac model shows a closer alignment with observed NO_2 levels, indicating that it may better represent the emission sources and dispersion processes in this location. The model's ability to more accurately simulate NO_2 concentrations here could be due to better representation of traffic-related emissions, which are a significant contributor to NO_2 levels.

In contrast, at the Cotocollao station, while the model successfully captures the temporal variability of NO_2, it tends to overestimate concentrations, especially during nighttime. This overestimation might be indicative of the model's heightened sensitivity to specific local factors, such as nighttime traffic or emissions from nearby sources that are less prominent during the day.

At the El Camal station, the BouLac model shows a balanced performance, capturing the overall trend of NO_2 concentrations. Although there is a slight underestimation of peak values, the model's ability to maintain a good overall agreement with observations indicates that it effectively represents the distribution of emissions at this station, despite some minor discrepancies.

For April, as shown in Fig. S3 and Table S7,† the BouLac model continues to deliver strong performance compared to the other models, maintaining its position as the best-performing model across different stations. While there is a general tendency to slightly underestimate NO_2 concentrations, particularly during certain times of the day, these results demonstrate the model's reliability and highlight areas where further refinement could enhance its accuracy.

The temporal evolution and concentration of NO_2 in urban environments are influenced not only by emission magnitudes but also by its photochemical coupling with ozone. Through the photo stationary cycle, freshly emitted NO reacts with ambient O_3 to form NO_2, and NO_2 is photolyzed under sunlight to regenerate O_3. In Quito, frequent cloudiness and topographic shading limit photolysis rates, especially during morning and evening hours, reducing the regeneration of O_3 and favoring NO_2 accumulation.[39]

The overestimation observed at stations such as Cotocollao may arise from limitations in the emissions inventory. Although the 2011 inventory disaggregates mobile sources by vehicle type (*e.g.*, taxis, buses, and light-duty vehicles), it does not account for differences in fleet age, EURO standards, or emission control technologies. These omissions can result in overestimated NO_x emissions, particularly in areas with lower-intensity traffic or newer vehicle fleets.[23,49]

No further calibration was applied beyond the meteorological sensitivity simulations presented in this study, as the objective was not to optimize a single model configuration but rather to assess the effect of different PBL schemes on pollutant concentrations. Nonetheless, the combined influence of local photochemical dynamics and structural characteristics of the emissions inventory is acknowledged as a contributor to model performance limitations for NO_2.

3.3 SO_2

Fig. 7 illustrates that all models predict temporal patterns for SO_2 similar to the observed data, particularly highlighting the afternoon underestimations. The simulations included (adjusted) annual emissions of 1500 ton per year for SO_2, which represent a 70% reduction with respect to the baseline emission (see further comments below). For December, this general alignment between models and observations suggests that the primary drivers of SO_2 concentrations—mainly industrial and energy-related point sources located in the city's southern and central areas, along with daytime boundary layer evolution and mixing processes—are reasonably represented in the simulations. The MYNN2 model consistently provided the best overall results for SO_2 across stations (Table S3†), making it the primary focus for this discussion.

At the Belisario and Carapungo stations, the MYNN2 model demonstrates a strong ability to track SO_2 levels, with both stations showing a similar pattern of slight underestimation during peak events. This underestimation might indicate that transient pollution events, likely linked to local activities, are not fully captured, yet the model still effectively represents the overall SO_2 trends.

In the case of El Camal and Cotocollao stations, the MYNN2 model encounters more variability in performance, particularly during periods of higher SO_2 concentrations. At the Guamaní station, the MYNN2 model shows performance like the case of Cotocollao, with some underestimation of SO_2 levels, particularly during peak periods. Although there is a tendency to underestimate peaks, the model still maintains a good alignment with the general trends observed at these stations.

For the month of April (Fig. S3 and Table S8†), the models continue to predict similar temporal patterns to the observations, again with some underestimation in the afternoon. The MYNN2 model maintains its position as the best-performing configuration, though the YSU model also proves to be a viable alternative, particularly during the morning and night hours when it shows closer alignment with observed SO_2 levels. This suggests that while MYNN2 is generally robust, YSU could offer additional insights, especially in scenarios where diurnal variations are critical.

In 2011, fuels distributed in Ecuador had high sulfur content. Based on the national fuel standard NTE INEN 935, Extra and Ecopaís gasoline contained up to 650 ppm of sulfur, Super gasoline up to 450 ppm, and premium diesel up to 500 ppm.[38] These values are significantly higher than international standards such as Euro V, which restricts sulfur content to 10 ppm. As a result, the combustion of these fuels likely
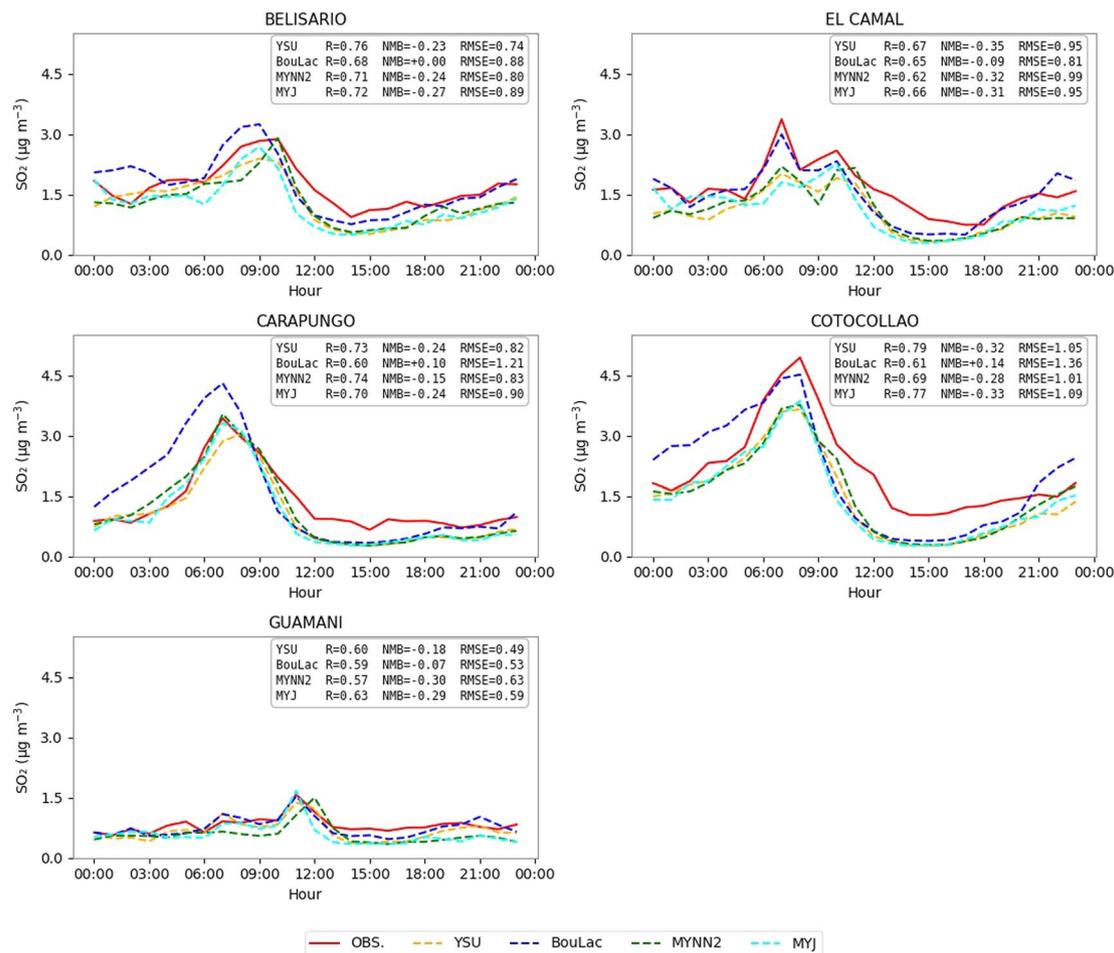
1322 | *Environ. Sci.: Adv.*, 2025, **4**, 1310–1332

© 2025 The Author(s). Published by the Royal Society of Chemistry

Fig. 7 Hourly average SO_2 concentrations at selected monitoring stations in Quito during December. The figure compares observed data (red solid line) with model simulations using four planetary boundary layer (PBL) schemes: YSU, MYJ, MYNN2, and BouLac. The curves represent daily averages by hour and are used to assess each configuration's ability to reproduce the diurnal cycle of SO_2. Statistical performance indicators (MB, NMB, RMSE, and r) are shown in each panel for each model.

contributed to elevated SO_2 levels in urban areas during the study period. Although sulfur content in diesel was reduced to 50 ppm starting in 2018 through regulatory improvements,[90] these changes occurred after the base year of the emissions inventory used in this study.[23] Our simulation results suggest that the SO_2 emissions reduction achieved in 2018 was ~70% with respect to the 2011 baseline.

Regarding source contributions, mobile sources were the dominant contributors to SO_2 emissions in Quito according to the 2011 emissions inventory. However, stationary sources, particularly industrial combustion and thermoelectric plants, also played a relevant role in specific areas, especially in the southern and industrial zones of the city.[91]

Due to Quito's complex topography and its location within a narrow Andean valley, atmospheric circulation is often constrained, particularly under stable conditions. These features may limit pollutant dispersion and promote the accumulation of locally emitted SO_2. While regional or long-range transport from external industrial sources or volcanoes could also influence background levels, such contributions were not explicitly

evaluated in this study. This is consistent with the study's objective, which focused on evaluating the impact of local emissions within the urban domain. Nevertheless, future research should incorporate chemical tracers or back-trajectory modeling to better quantify potential transboundary SO_2 influences.

3.4 O_3

All models successfully captured the general temporal patterns of ozone (O_3) across the different monitoring stations, demonstrating a strong ability to represent the diurnal variation in ozone levels. However, the BouLac model consistently stood out, providing the best overall performance across stations and seasons.

For December (as shown in Fig. 8 and supported by the hourly concentrations in Fig. S8† and statistical results in Table S4†), the BouLac model displayed a strong alignment with observed data at most stations. At the Belisario, Carapungo, and El Camal stations, the model slightly overestimated O_3 concentrations, particularly during the midday and early
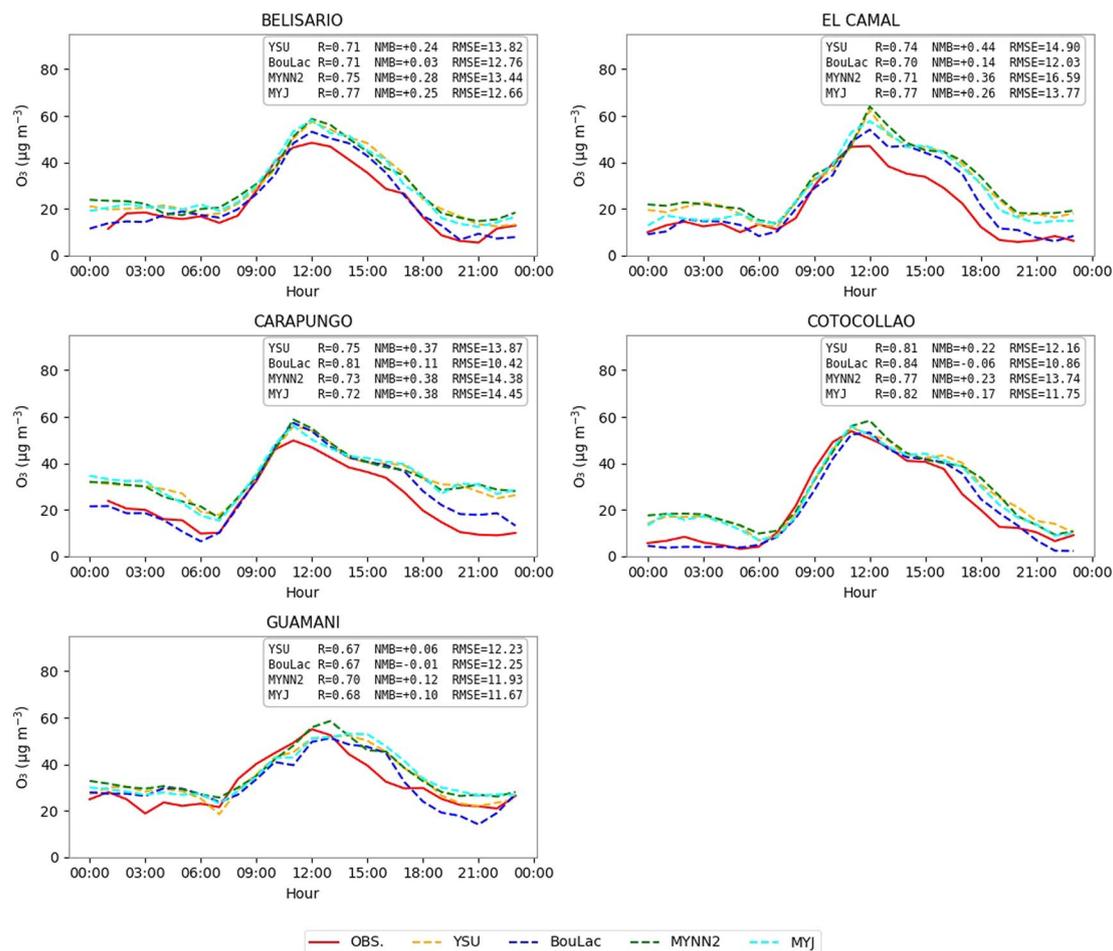
Fig. 8 Hourly average O_3 concentrations at selected monitoring stations in Quito during December. The figure compares observed data (red solid line) with model simulations using four planetary boundary layer (PBL) schemes: YSU, MYJ, MYNN2, and BouLac. The curves represent daily averages by hour and are used to assess each configuration's ability to reproduce the diurnal cycle of O_3. Statistical performance indicators (MB, NMB, RMSE, and r) are shown in each panel for each model.

afternoon peaks. Despite these minor overestimations, the model effectively captured the overall daily cycles and fluctuations, highlighting its capability to simulate the key processes influencing ozone levels.

In contrast, at the Cotocollao and Guamaní stations, the BouLac model tended to underestimate the O_3 peaks, particularly in the late afternoon and evening. Although these underestimations are observed, the model still managed to track the general trends and maintain a reasonable correlation with the observed data.

For April (as shown in Fig. S5† and supported by the hourly concentrations in Fig. S7† and statistical results in Table S10†), the BouLac model continued to perform robustly across all stations. The patterns observed in December were consistent in April, with the model slightly overestimating ozone levels at Belisario, Carapungo, and El Camal, while slightly underestimating them at Cotocollao and Guamaní. This consistency across different months underscores the model's reliability for simulating ozone levels under varying seasonal conditions in Quito.

3.5 PM$_{2.5}$

The analysis of PM$_{2.5}$ concentrations indicates that while there is a general tendency among all models to slightly underestimate observed levels, the BouLac model consistently demonstrated the closest alignment with the observed data across all monitoring stations. This strong performance is particularly evident during peak pollution hours, both in December and April.

In December (Fig. 9 and Table S5†), the BouLac model showed a balanced performance across the stations. At the Belisario and Cotocollao stations, the model slightly overestimated PM$_{2.5}$ concentrations. Despite this overestimation, the model effectively captured the temporal patterns and general pollution trends, indicating a reliable performance in these areas.

Conversely, at the El Camal and Guamaní stations, the BouLac model tended to underestimate PM$_{2.5}$ levels, especially during higher pollution events. The Carapungo station presented the most significant underestimations, particularly during peak pollution periods. Although the model faced
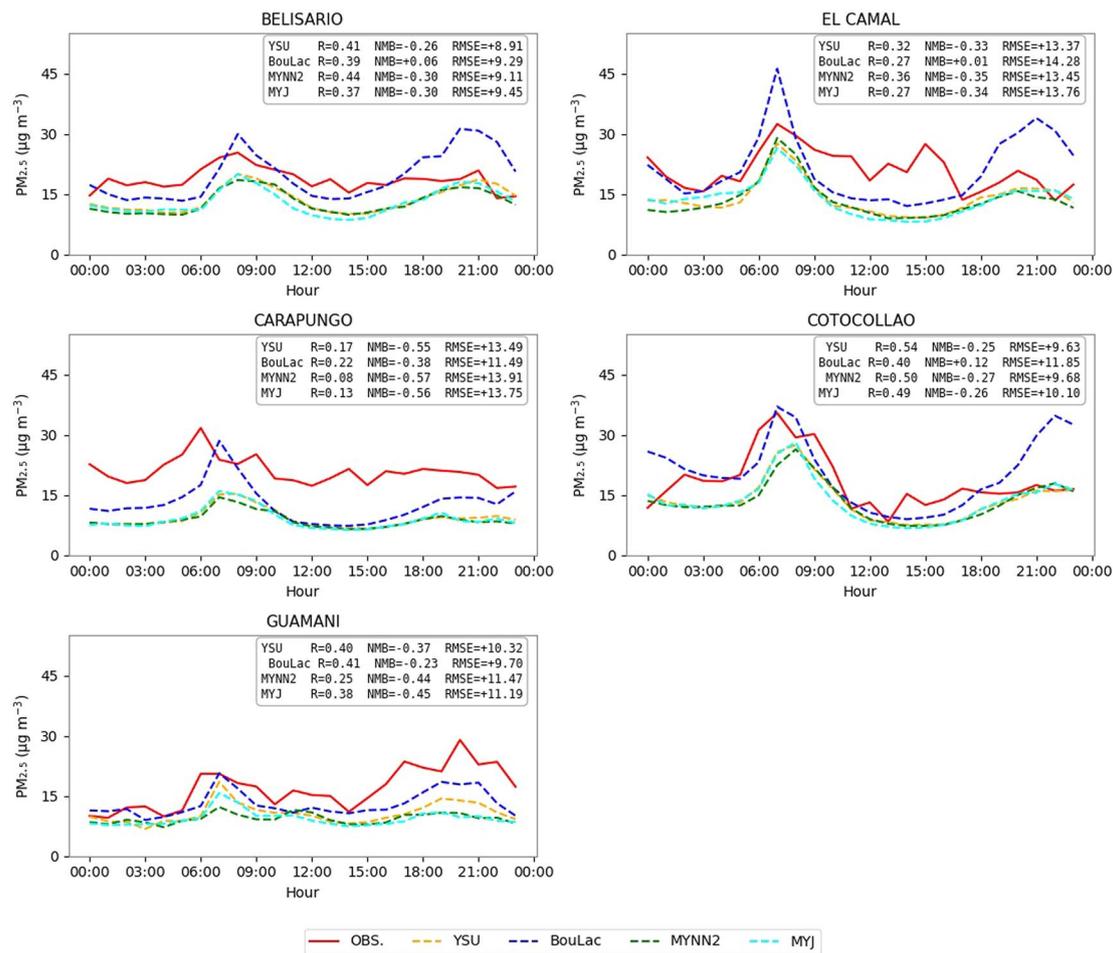
Fig. 9 Hourly average $PM_{2.5}$ concentrations at selected monitoring stations in Quito during December. The figure compares observed data (red solid line) with model simulations using four planetary boundary layer (PBL) schemes: YSU, MYJ, MYNN2, and BouLac. The curves represent daily averages by hour and are used to assess each configuration's ability to reproduce the diurnal cycle of $PM_{2.5}$. Statistical performance indicators (MB, NMB, RMSE, and r) are shown in each panel for each model.

challenges in accurately capturing extreme events here, it still provided a consistent representation of the broader $PM_{2.5}$ trends.

For April (Fig. S6 and Table S10†), the BouLac model once again emerged as the best-performing configuration, maintaining a strong correlation with observed $PM_{2.5}$ levels across all stations. The trends observed in December were largely mirrored in April, with the model continuing to exhibit a slight overestimation at Belisario and Cotocollao, and underestimations at El Camal, Guamaní, and Carapungo.

To understand the present performance for $PM_{2.5}$ modeling in Quito, we discuss related results here. According to Jat *et al.*,[88] the CB05-MADE/SORGAM chemical mechanism—one that has improvements with respect to the CBMZ mechanism used here—had a systematic underestimation of $PM_{2.5}$ concentrations, particularly during high pollution events in Delhi. The analysis of this model revealed a mean bias (MB) of −7.69, a normalized mean bias (NMB) of −0.38, a normalized mean gross error (NMGE) of 0.56, and a root mean square error (RMSE) of 11.49 at certain stations, indicating significant errors in predicting extreme events. However, this model successfully

captured the general pollution trends, as reflected by a moderate correlation of 0.22. These findings are consistent with the results obtained from monitoring stations in Quito, where a similar systematic underestimation of $PM_{2.5}$ concentrations was observed across the entire diurnal cycle. This persistent bias is evident at all stations and is not limited to high pollution peaks, as shown in Fig. 9.

It is important to note that this underestimation does not seem to be due to other area sources, as the traffic inventory is quite high and is the dominant area source in Quito. From a receptor modeling standpoint, a recent study[92] estimated a source apportionment of carbonaceous aerosols in several South American cities, including Quito. For Quito, secondary organic aerosol (SOA) and regional biomass burning aerosols (BBOA) contributed 20% and 21% of total organic carbon, respectively. Thus, this means that the models' underestimation of $PM_{2.5}$ may be ascribed to (a) not including regional biomass burning emissions in the modeling, and (b) the MADE/SORGAM mechanism underestimates SOA formation, which is a known issue.

© 2025 The Author(s). Published by the Royal Society of Chemistry

Environ. Sci.: Adv., 2025, **4**, 1310–1332 | **1325**

While precipitation effects were reasonably captured—evidenced by the consistent drop in concentrations during rainfall events—the persistent underestimation of PM$_{2.5}$ under dry conditions suggests that wash-out is not the sole missing process. Although this study does not provide a figure explicitly comparing dry and wet conditions, the temporal patterns shown in Fig. 9 and S6† indicate that underestimations persist regardless of rainfall. This suggests that additional sources not represented in the emissions inventory may contribute to the observed bias. Additionally, a significant drop in PM$_{2.5}$ concentrations during the 2019 national strike,[93] when traffic was reduced, underscores the relevance of mobile sources. Additional simulations were conducted including regional biomass burning emissions (in domains 1 and 2) from the FINN2.5 inventory and varying the vertical plume injection profile. These scenarios showed small changes in hourly PM$_{2.5}$ concentrations at the urban monitoring stations (ESI Fig. S9 and S10†), suggesting that the underestimation is primarily linked to local sources and atmospheric processes. Hence, underestimation of local emissions and of SOA formation are a plausible explanation for the persistent model underestimation of PM$_{2.5}$.

3.6 Analysis of observed *vs.* modeled air pollutant concentrations in Quito

Fig. 10 provides a summary of the observed and modeled average concentrations in Quito for the month of December. Fig. S11 in the ESI† extends this analysis to include the month of April. The comparison between observed and modeled data reveals both successes and limitations in the accuracy of the air quality models used and highlights areas where local sources may not be accurately included in emission inventories. For CO, observed and modeled concentrations show a strong agreement, suggesting that the primary sources of CO, such as vehicular emissions, are well represented in the model input emissions. In contrast, for NO$_2$, the observed concentrations are consistently higher than the modeled ones.

This discrepancy suggests that specific local sources may be underrepresented in the emissions inventory. While the agreement between observed and modeled CO suggests that light-duty gasoline vehicle emissions are well characterized, NO$_2$ emissions are more strongly influenced by heavy-duty diesel vehicles and industrial sources. These sectors are more difficult to quantify due to uncertainties in fleet composition, emission factors, and spatial allocation. As such, the model may require
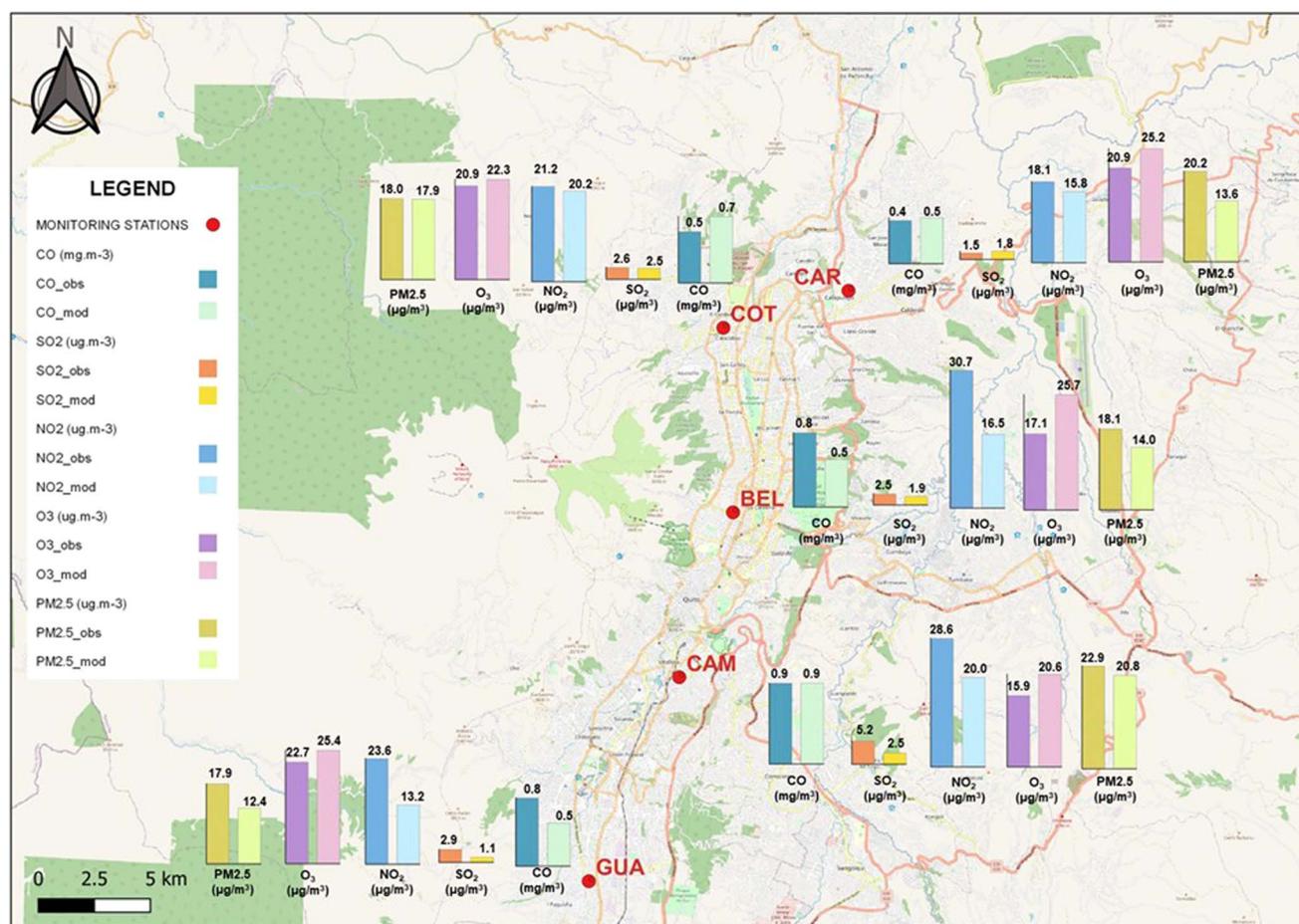

Fig. 10 Average pollutant concentrations: observed *vs.* modeled, December 2018.

further refinement of these specific NO_x emission sources to improve agreement with observed NO_2 levels.

Ozone (O_3) concentrations are quite similar among observed and modeled data, indicating that the models adequately represent the photochemical reactions and atmospheric conditions influencing ozone formation in the urban area of Quito. This similarity suggests a good capability of the model to predict the spatial distribution of ozone. We tested the effects of removing biogenic VOC emissions, and the model predictions were reduced in all configurations used, although the changes were smaller in magnitude.

We found that biogenic emissions contributed positively to ozone levels, with a 3.3% average increase in December and an 8% increase in April. This seasonal variability is influenced by environmental factors such as temperature and solar radiation, which are higher in April, leading to increased production of biogenic VOCs. These findings are consistent with global research indicating the crucial role of these VOCs, particularly isoprene and monoterpenes, which are the most abundant and reactive biogenic compounds emitted by vegetation. These compounds react rapidly in the presence of nitrogen oxides (NO_x) and sunlight, contributing significantly to ozone formation in the troposphere.[94,95] In regions with similar climates and vegetation, biogenic emissions are significantly higher during warm months.[96] For example, in some studies, biogenic emissions have been estimated to contribute an average of 12% to ozone production during summer, with this percentage increasing up to 60% during heatwaves.[97]

Inclusion of aerosol radiative effects brought smaller changes in ozone, because simulated ambient $PM_{2.5}$ concentrations were low. In our model, removing the radiative effects of aerosols resulted in a decrease of less than 0.5% in average ozone concentrations for both December and April. This marginal change aligns with findings in tropical regions such as Ecuador, where the impact of aerosol radiative effects on ozone formation is generally less pronounced due to the relatively lower concentrations of ambient aerosols compared to other regions.[97]

All model configurations tested underestimated observed $PM_{2.5}$ concentrations. These results are mainly ascribed to the underestimation of secondary aerosol formation, which is a known issue in the MADE/SORGAM aerosol module.[98] These results highlight the need to improve emission inventories and test other aerosol models to better capture $PM_{2.5}$ dynamics in Quito.

4 Conclusions

Despite limitations in local data availability and emission characterization—particularly for secondary organic aerosol formation, VOCs, and non-exhaust $PM_{2.5}$ sources—this study presents a robust and technically sound evaluation of air quality in Quito. The model's performance across multiple pollutants and scenarios demonstrates that meaningful, policy-relevant insights can still be extracted when using carefully adapted inventories and advanced modeling tools. Rather than weakening the findings, the identified data gaps provide direction for future improvements and highlight the importance of this

study as a foundational step toward operational forecasting and emission refinement in data-limited urban environments.

This study underscores both the potential and challenges of employing advanced air quality modeling techniques in a complex urban environment such as Quito. While the WRF-Chem model demonstrates effectiveness in simulating ozone, CO, NO_2 and SO_2, limitations arise in accurately modeling $PM_{2.5}$ concentrations mainly to an underestimation of SOA concentrations in the aerosol module used. SO_2 is a challenging species to model due to a lack of detailed information on stack source parameters. The absence of ambient VOC and NH_3 measurements hampers efforts to refine emission estimates, which is another limitation in the present study.

This research demonstrates the substantial updates made to the 2011 local emissions inventory, which were only possible through the application of an advanced chemical transport model such as WRF-Chem. These improvements addressed critical gaps in previous estimates, such as the significant underestimation of $PM_{2.5}$ emissions. By leveraging advanced modeling techniques, the updated inventory now provides a more accurate representation of emission sources, better reflecting local conditions and dynamics in Quito. These enhancements emphasize the importance of integrating high-resolution modeling tools with localized data to refine emission inventories and improve air quality predictions.

This study highlights the fundamental need for high-resolution, region-specific emission inventories to enhance air quality predictions and reduce modeling discrepancies in complex urban environments. Accurate characterization of key emission sources—such as traffic, industrial activities, and biomass burning—is essential for improving the simulation of primary and secondary pollutants. Future efforts should prioritize the inclusion of ambient measurements of volatile organic compounds (VOCs) and ammonia (NH_3), which play a critical role in the formation of secondary pollutants and remain uncertain in current inventories. By addressing these gaps, policymakers can develop more effective air quality regulations and interventions tailored to the specific challenges of cities such as Quito. This study marks a pivotal advancement in air quality modeling for Andean cities such as Quito, offering a comprehensive framework that bridges the gap between global atmospheric models and localized data. By integrating high-resolution emission inventories, advanced chemical mechanisms, and dynamic meteorological modeling within the WRF-Chem framework, this research provides actionable insights into the complex interplay of urban emissions and atmospheric processes in tropical mountainous regions. Beyond its technical contributions, the study underscores the necessity of coupling scientific modeling with robust observational data and policy frameworks to address urban air quality challenges effectively. This integrated approach not only enhances our understanding of pollutant dynamics in cities with unique topographical and climatic conditions but also lays the groundwork for evidence-based interventions that safeguard public health and promote sustainable urban development. As such, this work contributes significantly to the state of the art, demonstrating a replicable

© 2025 The Author(s). Published by the Royal Society of Chemistry

Environ. Sci.: Adv., 2025, **4**, 1310–1332 | **1327**

methodology that can inform air quality management strategies across similar regions worldwide.

Author contributions

Gabriela Mancheno: data curation, visualization, investigation, writing – original draft & review. Héctor Jorquera: conceptualization, software, formal analysis, methodology, investigation, writing – final draft and editing.

Conflicts of interest

On behalf of all authors, the corresponding author states that there are no conflicts of interests.

References

1 Ministerio de Ambiente Ecuador, Programa Calidad del Aire, 2020, retrieved from **https://www.ambiente.gob.ec/programa-calidad-del-aire-fase-iii/**.

2 Programa de las Naciones Unidas para el Medio Ambiente (PNUMA) and Ministerio de Ambiente (MAE) y Facultad Latinoamericana de Ciencias Sociales (FLACSO), *GEOECUADOR*, 2008, retrieved from: **https://biblio.flacsoandes.edu.ec/libros/digital/41444.pdf**.

3 J. Franco, L. Gidhagen, R. Morales and E. Behrentz, Towards a better understanding of urban air quality management capabilities in Latin America, *Environ. Sci. Policy*, 2019, **102**, 43–53, DOI: **10.1016/j.envsci.2019.09.011**.

4 Instituto Nacional de Estadística y Censos, *Ficha cantonal Distrito Metropolitano de Quito*, 2015, retrieved from: **https://www.ecuadorencifras.gob.ec/documentos/web-inec/Estadisticas_territoriales/Estadisticas_Cantonales/Pichincha/quito.pdf**.

5 V. Valencia, O. Hertel, M. Ketzel and G. Levin, Modeling urban background air pollution in Quito, Ecuador, *Atmos. Pollut. Res.*, 2020, **11**(4), 646–666, DOI: **10.1016/j.apr.2019.12.014**.

6 Secretaría de Ambiente, 2020, **http://www.quitoambiente.gob.ec/**.

7 M. Gavidia-Calderón, A. Vara-Vela, N. Crespo and M. Andrade, Impact of time-dependent chemical boundary conditions on tropospheric ozone simulation with WRF-Chem: An experiment over the Metropolitan Area of São Paulo, *Atmos. Environ.*, 2018, **195**, 112–124, DOI: **10.1016/j.atmosenv.2018.09.026**.

8 D. Pellegatti, M. Andrade, R. Ynonue and J. Ching, Effect of Local Climate Zone (LCZ) classification on ozone chemical transport model simulations in Sao Paulo, Brazil, *Urban Clim.*, 2019, **27**, 293–313, DOI: **10.1016/j.uclim.2018.12.007**.

9 C. González, R. Ynoue, A. Vara-Vela, N. Rojas and B. Aristizábal, High-resolution air quality modeling in a medium-sized city in the tropical Andes: Assessment of local and global emissions in understanding ozone and PM10 dynamics, *Atmos. Pollut. Res.*, 2018, **9**(5), 934–948, DOI: **10.1016/j.apr.2018.03.003**.

10 H. Navarro and A. Luna, Simulation and Evaluation of PM10 in the City of Lima Using the Model WRF-Chem, *Int. Proc. Chem., Biol. Environ. Eng.*, 2018, **103**, 47–54, DOI: **10.7763/IPCBEE**.

11 O. Sánchez-Ccoyllo, C. Ordoñez-Aquino, Á. Muñoz, A. Llacza, M. Andrade, Y. Liu, W. Reátegui-Romero and G. Brasseur, Modeling Study of the Particulate Matter in Lima with the WRF-Chem Model: Case Study of April 2016, *Int. J. Appl. Eng. Res.*, 2018, **13**(11), 10129–10141.

12 A. Moya-Álvarez, R. Estevan, S. Kumar, J. Flores, J. Ticse, D. Martínez-Castro and S. Yamina, Influence of PBL parameterization schemes in WRF_ARW model on short-range precipitation's forecasts in the complex orography of Peruvian Central Andes, *Atmos. Res.*, 2020, 104708, DOI: **10.1016/j.atmosres.2019.104708**.

13 M. Saavedra, C. Junquas, J. C. Espinoza and Y. Silva, Impacts of topography and land use changes on the air surface temperature and precipitation over the central Peruvian Andes, *Atmos. Res.*, 2020, **234**, 104711.

14 D. Moscoso-Vanegas, V. Vázquez and A. Astudillo, Modelamiento de la calidad del aire en la ciudad de Cuenca-Ecuador, *Iteckne*, 2015, **12**(2), 188–197. Retrieved from **http://www.scielo.org.co/scielo.php?script=sci_arttext&pid=S1692-17982015000200010&lng=en&tlng=es**.

15 R. Parra, Evaluación Preliminar de la Temperatura Media en Superficie del Ecuador para el año 2010, obtenida mediante el modelo Weather Research Forecasting (WRF), *Av. en Cienc. e Ing.*, 2012, **4**(2), C27–C35, DOI: **10.18272/aci.v4i2.110**.

16 R. Parra, Assessment of planetary boundary layer schemes of the WRF-Chem model in the simulation of carbon monoxide dispersion in the urban area of Quito, Ecuador, *WIT Trans. Ecol. Environ.*, 2017, **211**, 41–50, DOI: **10.2495/AIR170041**.

17 R. Parra, Performance studies of planetary boundary layer schemes in WRF-Chem for the Andean region of Southern Ecuador, *Atmos. Pollut. Res.*, 2018, **9**(3), 411–428, DOI: **10.1016/j.apr.2017.11.011**.

18 M. Cazorla and E. Tamayo, Atmospheric measurement station in Universidad San Francisco de Quito (EMA): ground-based physical meteorology instrumentation and

assessment of initial measurements, *Av. Cienc. Ing.*, 2014, **6**(2), C21–C30.

19 R. Zalakeviciute, R. Vasquez, D. Bayas, A. Buenano, D. Mejia, R. Zegarra, A. Diaz and B. Lamb, Drastic Improvements in Air Quality in Ecuador during the COVID-19 Outbreak, *Aerosol Air Qual. Res.*, 2020, **20**, 1783–1792, DOI: **10.4209/aaqr.2020.05.0254**.

20 W. C. Skamarock, J. B. Klemp, J. Dudhia, D. O. Gill, Z. Liu, J. Berner, W. Wang, J. G. Powers, M. G. Duda and D. M. Barker, *A Description of the Advanced Research WRF Model Version 4*, National Center for Atmospheric Research, Boulder, CO, USA, 2019, p. 145.

21 M. Guevara, C. Tena, M. Porquet, O. Jorba and C. Pérez, HERMESv3, a stand-alone multi-scale atmospheric emission modelling framework – Part 1: global and regional module, *Geosci. Model Dev.*, 2019, **12**, 1885–1907, DOI: **10.5194/gmd-12-1885-2019**.

22 V. H. Valencia, O. Hertel, M. Ketzel and G. Levin, Modeling urban background air pollution in Quito, Ecuador, *Atmos. Pollut. Res.*, 2020, **11**(4), 646–666.

23 J. Baca, *Informe Final Inventario de Emisiones de Contaminantes Criterio, DMQ 2011*, Secretaría de Ambiente del Distrito Metropolitano de Quito, 2014.

24 Secretaría General de Coordinación Territorial y Participación Ciudadana, Información sobre zonales, 2023, retrieved from **https://zonales.quito.gob.ec/?page_id=16401**.

25 World Meteorological Organization (WMO), Towards Integrated Urban Weather, Environment and Climate Services. Bulletin No. 63 (1), 2014, retrieved from **https://public.wmo.int/en/resources/bulletin/towards-integrated-urban-weather-environment-and-climate-services**.

26 INEC, Proyecciones Poblacionales, Instituto Nacional de Estadísticas y Censos [Sitio web], URL, 2023, **https://www.ecuadorencifras.gob.ec/proyecciones-poblacionales/**, accessed on March 17, 2024.

27 INEC, Ecuador - VII Censo de Población y VI de Vivienda 2010, Información General [Sitio web], URL, 2018, **https://anda.inec.gob.ec/anda/index.php/catalog/659**, accessed on November 6, 2024.

28 V. H. Valencia, G. Levin and M. Ketzel, Densification versus urban sprawl. Modeling the impact of two urban growth scenarios on air quality, *Atmos. Environ.*, 2023, **310**, 119963, DOI: **10.1016/j.atmosenv.2023.119963**.

29 Instituto Nacional de Meteorología e Hidrología del Ecuador (INAMHI), Pronóstico del tiempo, 2021, **https://www.inamhi.gob.ec/pronostico-del-tiempo-y-productos/**.

30 A. R. Berne, S. R. Vieira and A. H. andMaia, Urban climate variability in Quito, Ecuador, *Int. J. Climatol.*, 2002, **22**(11), 1377–1392, DOI: **10.1002/joc.808**.

31 V. Díaz-Suárez, F. Baraldo Victorica, P. Lichtig, M. Díaz Resquin, M. Vargas-Rojas, J. Murillo-Hernández, J. A. Vergara Correa, M. de Fatima Andrade, D. Monteiro dos Santos, J. Flores Maldonado, F. Aldape, L. F. Abreu and M. I. andManousakas, Carbonaceous fraction in PM2.5 of six Latin American cities: Seasonal variations, sources and secondary organic carbon contribution, *Sci. Total Environ.*, 2024, **948**, 174630, DOI: **10.1016/j.scitotenv.2024.174630**.

32 K. Alexandrino, M. Gavidia-Calderón, A. Cazorla and D. Rodríguez, Seasonal variation of the criteria air pollutants concentration in an urban area of a high-altitude city, *Proceedings of the 11th International Conference on Air Quality – Science and Application*, 2020. **https://www.researchgate.net/publication/343405559**.

33 Global Volcanism Program, *Ecuador Volcanoes*, Smithsonian Institution, recuperado de **https://volcano.si.edu/volcanolist_countries.cfm?country=Ecuador**.

34 J. C. Rubio Terán, J. S. Cueva Reyes and O. E. Carrera Enríquez, Evolution of air quality as a function of vehicle demand in the Metropolitan District of Quito, *Espir. Multidiscip. Res. J.*, 2024, **8**(4)). Retrieved from **https://www.revistaespirales.com/index.php/es/article/view/874**.

35 P. E. Carrillo, A. S. Malik and Y. Yoo, Driving restrictions that work? Quito's Pico y Placa Program, *Can. J. Econ.*, 2016, **49**(4), 1536–1568. Retrieved from **https://www.researchgate.net/publication/311356603_Driving_restrictions_that_work_Quito's_Pico_y_Placa_Program**.

36 L. R. Jacome Galarza, W. E. Jaramillo Sangurima and S. A. Jaramillo Luzuriaga, Traffic congestion in Ecuador: A comprehensive review, key factors, impact, and solutions of smart cities, *Lat. Am. J. Computing*, 2025, **12**(1)). Retrieved from **https://lajc.epn.edu.ec/index.php/LAJC/article/view/419**.

37 P. G. Boulter, J. Borken-Kleefeld and L. Ntziachristos, The evolution and control of NOx emissions from road transport in Europe, In *Urban air quality in Europe*, ed. M. Viana, Springer, 2012, pp. 31–53, **https://www.researchgate.net/publication/278658669_The_Evolution_and_Control_of_NOx_Emissions_from_Road_Transport_in_Europe**.

38 Cámara de Industrias y Producción (CIP), Contenido de azufre en combustibles utilizados en Ecuador, 2013, retrieved from: **https://www.cip.org.ec/**.

39 M. Cazorla, Air quality over a populated Andean region: insights from measurements of ozone, NO, and boundary layer depths, *Atmos. Pollut. Res.*, 2016, **7**, 66–74, DOI: **10.1016/J.APR.2015.07.006**.

40 C. I. Alvarez-Mendoza, A. Teodoro, A. Freitas and J. Fonseca, Spatial estimation of chronic respiratory diseases based on machine learning procedures—An approach using remote sensing data and environmental variables in Quito, Ecuador, *Appl. Geogr.*, 2020, **123**, 102273.

41 CORPAIRE, *Inventario de Emisiones del Distrito Metropolitano de Quito 2003*, 2006.

42 CORPAIRE, *Inventario de Emisiones del Distrito Metropolitano de Quito 2005*, 2008.

43 CORPAIRE, *Inventario de Emisiones del Distrito Metropolitano de Quito 2007*, 2009.

44 Secretaría de Ambiente, *Inventario de Emisiones del Distrito Metropolitano de Quito 2009*, Secretaría de Ambiente del Distrito Metropolitano de Quito, Quito, Ecuador, 2011.

© 2025 The Author(s). Published by the Royal Society of Chemistry

Environ. Sci.: Adv., 2025, **4**, 1310–1332 | **1329**

45 CORPAIRE, *Inventario de emisiones de contaminantes criterio, DMQ 2011*, Secretaría de Ambiente del Distrito Metropolitano de Quito, 2014.

46 EPPetroecuador, *Despachos mensuales de combustible 2011*, Archivos Internos, 2010.

47 R. León and F. Godoy, *Modelo de Tráfico del Distrito Metropolitano de Quito, año 2005*, Dirección Metropolitana de Transporte, 2004.

48 Secretaría de Ambiente, Reportes de caracterización físico-química de emisiones gaseosas, *Dirección de Control Ambiental del DMQ*, 2014.

49 D. Vega, L. Ocaña and R. Parra Narváez, On-road traffic air pollutants emission inventory in the Distrito Metropolitano de Quito. Base year 2012, *ACI Avances en Ciencias e Ingenierías (Quito)*, 2015, **7**(2), 71–78, DOI: **10.18272/aci.v7i2.270**.

50 Ministerio del Ambiente del Ecuador, Summary of the National Greenhouse Gas Inventory of Ecuador, Time Series 1994–2012, Quito, Ecuador, 2016, retrieved from **https://info.undp.org/docs/pdc/Documents/ECU/06ResumenEjecutivoINGEIdeEcuador.SerieTemporal1994-2012.pdf**.

51 M. Crippa, D. Guizzardi, T. Butler, T. Keating, R. Wu, J. Kaminski, J. Kuenen, J. Kurokawa, S. Chatani, T. Morikawa, G. Pouliot, J. Racine, M. D. Moran, Z. Klimont, P. M. Manseau, R. Mashayekhi, B. H. Henderson, S. J. Smith, H. Suchyta, M. Muntean, E. Solazzo, M. Banja, E. Schaaf, F. Pagani, J.-H. Woo, J. Kim, F. Monforti-Ferrario, E. Pisoni, J. Zhang, D. Niemi, M. Sassi, T. Ansari and K. Foley, The HTAP_v3 emission mosaic: Merging regional and global monthly emissions (2000–2018) to support air quality modelling and policies, *Earth Syst. Sci. Data*, 2023, **15**, 2667–2694, DOI: **10.5194/essd-15-2667-2023**.

52 W. Skamarock, J. Klemp, J. Dudhia, D. Gill, D. Barker, M. Duda, X.-Y. Huang, W. Wang and J. Powers, *A Description of the Advanced Research WRF Version 3, NCAR Technical Note*, 2008.

53 W. C. Skamarock, J. B. Klemp, J. Dudhia, D. O. Gill, Z. Liu, J. Berner, W. Wang, J. G. Powers, M. G. Duda, D. Barker and X.-y. Huang, *A Description of the Advanced Research WRF Model Version 4.3 [Technical Report]*, 2021, retrieved from DOI: **10.5065/1dfh-6p97**.

54 M. Guevara, C. Tena, M. Porquet, O. Jorba and C. Pérez García-Pando, HERMESv3, a stand-alone multi-scale atmospheric emission modelling framework – Part 2: The bottom–up module, *Geosci. Model Dev.*, 2020, **13**, 873–903, DOI: **10.5194/gmd-13-873-2020**.

55 Agencia Metropolitana de Tránsito (AMT), 2020, **https://www.amt.gob.ec/**.

56 G. A. Grell, S. Peckham, R. Schmitz, S. McKeen, G. Frost, W. Skamarock and B. Eder, Fully coupled "online" chemistry within the WRF model, *Atmos. Environ.*, 2005, **39**(37), 6957–6975, DOI: **10.1016/j.atmosenv.2005.04.027**.

57 National Centers for Environmental Prediction, National Weather Service, NOAA and U.S. Department of Commerce, NCEP GDAS/FNL 0.25 Degree Global Tropospheric Analyses and Forecast Grids, *Research Data Archive at the National Center for Atmospheric Research*, Computational and Information Systems Laboratory, Boulder, CO, 2015, DOI: **10.5065/D65Q4T4Z**.

58 D. Byun and K. L. Schere, Review of the governing equations, computational algorithms, and other components of the Models-3 Community Multiscale Air Quality (CMAQ) modeling system, *Appl. Mech. Rev.*, 2006, **59**(2), 51–77, DOI: **10.1115/1.2128636**.

59 L. Menut, B. Bessagnet, D. Khvorostyanov, M. Beekmann, N. Blond, A. Colette, R. Vautard, *et al.*). CHIMERE 2013: a model for regional atmospheric composition modelling, *Geosci. Model Dev.*, 2013, **6**(4), 981–1028, DOI: **10.5194/gmd-6-981-2013**.

60 R. R. Draxler and G. D. Hess, An overview of the HYSPLIT_4 modelling system for trajectories, dispersion and deposition, *Aust. Meteorol. Mag.*, 1998, **47**, 295–308.

61 M. Cazorla and J. Juncosa, Planetary boundary layer evolution over an equatorial Andean valley: A simplified model based on balloon-borne and surface measurements, *Atmos. Sci. Lett.*, 2018, **19**(8), 1–7, DOI: **10.1002/asl.829**.

62 S.-Y. Hong, Y. Noh and J. Dudhia, A new vertical diffusion package with an explicit treatment of entrainment processes, *Mon. Weather Rev.*, 2006, **134**(9), 2318–2341, DOI: **10.1175/MWR3199.1**.

63 Z. I. Janjić, The step-mountain eta coordinate model: Further developments of the convection, viscous sublayer, and turbulence closure schemes, *Mon. Weather Rev.*, 1994, **122**(5), 927–945, DOI: **10.1175/1520-0493(1994)122<0927:TSMECM>2.0.CO;2**.

64 M. Nakanishi and H. Niino, An improved Mellor–Yamada Level-3 model: Its numerical stability and application to a regional prediction of advection fog, *Boundary-Layer Meteorol.*, 2006, **119**(2), 397–407, DOI: **10.1007/s10546-005-9030-8**.

65 S.-Y. Hong and J.-O. J. Lim, The WRF single-moment 6-class microphysics scheme (WSM6), *J. Kor. Meteorol. Society*, 2006, **42**(2), 129–151.

66 M. J. Iacono, J. S. Delamere, E. J. Mlawer, M. W. Shephard, S. A. Clough and W. D. Collins, Radiative forcing by long-lived greenhouse gases: Calculations with the AER radiative transfer models, *J. Geophys. Res.:Atmos.*, 2008, **113**, D13103, DOI: **10.1029/2008JD009944**.

67 C. A. Paulson, The mathematical representation of wind speed and temperature profiles in the unstable atmospheric surface layer, *J. Appl. Meteorol. Climatol.*, 1970, **9**(6), 857–861, DOI: **10.1175/1520-0450(1970)009<0857:TMROWS>2.0.CO;2**.

68 A. J. Dyer and B. B. Hicks, Flux-gradient relationships in the constant flux layer, *Q. J. R. Metereol. Soc.*, 1970, **96**(410), 715–721, DOI: **10.1002/qj.49709641012**.

69 E. K. Webb, Profile relationships: The log-linear range, and extension to strong stability, *Q. J. R. Metereol. Soc.*, 1970, **96**(407), 67–90, DOI: **10.1002/qj.49709640708**.

70 P. A. Jiménez, J. Dudhia, J. F. González-Rouco, J. Navarro, J. P. Montávez and E. García-Bustamante, A revised scheme for the WRF surface layer formulation, *Mon.*

1330 | *Environ. Sci.: Adv.*, 2025, **4**, 1310–1332

© 2025 The Author(s). Published by the Royal Society of Chemistry

Weather Rev., 2012, **140**(3), 898–918, DOI: **10.1175/MWR-D-11-00056.1**.

71 M. Tewari, F. Chen, W. Wang, J. Dudhia, M. A. LeMone, K. Mitchell, G. Gayno, *et al.*, Implementation and verification of the unified NOAH land surface model in the WRF model, *Proceedings of the 20th Conference on Weather Analysis and Forecasting/16th Conference on Numerical Weather Prediction*, 2004, **https://www2.mmm.ucar.edu/wrf/users/docs/presentation_wof/Tewari.pdf**.

72 A. Martilli, A. Clappier and M. W. Rotach, An urban surface exchange parameterisation for mesoscale models, *Boundary-Layer Meteorol.*, 2002, **104**(2), 261–304, DOI: **10.1023/A:1016099921195**.

73 G. A. Grell and D. Dévényi, A generalized approach to parameterizing convection combining ensemble and data assimilation techniques, *Geophys. Res. Lett.*, 2002, **29**(14), 38, DOI: **10.1029/2002GL015311**.

74 W. R. Stockwell, P. Middleton, J. S. Chang and X. Tang, The second generation regional acid deposition model chemical mechanism for regional air quality modeling, *J. Geophys. Res.:Atmos.*, 1990, **95**(D10), 16343–16367, DOI: **10.1029/JD095iD10p16343**.

75 I. J. Ackermann, H. Hass, M. Memmesheimer, A. Ebel, F. S. Binkowski and U. Shankar, Modal aerosol dynamics model for Europe: Development and first applications, *Atmos. Environ.*, 1998, **32**(17), 2981–2999, DOI: **10.1016/S1352-2310(98)00006-5**.

76 B. Schell, I. J. Ackermann, H. Hass, F. S. Binkowski and A. Ebel, Modeling the formation of secondary organic aerosol within a comprehensive air quality model system, *J. Geophys. Res.:Atmos.*, 2001, **106**(D22), 28275–28293, DOI: **10.1029/2001JD000384**.

77 G. Janssens-Maenhout, M. Crippa, D. Guizzardi, F. Dentener, M. Muntean, G. Pouliot, T. Keating, Q. Zhang, J. Kurokawa, R. Wankmüller, H. Denier van der Gon, J. J. P. Kuenen, Z. Klimont, G. Frost, S. Darras, B. Koffi and M. Li, HTAP_v2.2: A mosaic of regional and global emission grid maps for 2008 and 2010 to study hemispheric transport of air pollution, *Atmos. Chem. Phys.*, 2015, **15**(19), 11411–11432, DOI: **10.5194/acp-15-11411-2015**.

78 W. Wang, D. Barker, C. Bruyère, C. Duda, J. Dudhia, D. Gill, J. Michalakes and S. Rizvi, *WRF Version 3 Modeling System User's Guide*, 2008, retrieved from **http://www.mmm.ucar.edu/wrf/users/docs/userguideV3/**.

79 W. Cheng and W. Steenburgh, Evaluation of surface sensible weather forecasts by the WRF and the Eta model over the western United States, *Weather Forecast.*, 2005, **20**, 812–821, DOI: **10.1175/WAF885.1**.

80 S. Falasca, I. Gandolfi, S. Argentini, F. Barnaba, G. Casasanta, L. Di Liberto, I. Petenko and G. Curci, Sensitivity of near-surface meteorology to PBL schemes in WRF simulations in a port-industrial area with complex terrain, *Atmos. Res.*, 2021, **264**, 105824, DOI: **10.1016/j.atmosres.2021.105824**.

81 N. Chaouch, M. Temimi, M. Weston and H. Ghedira, Sensitivity of the meteorological model WRF-ARW to

planetary boundary layer schemes during fog conditions in a coastal arid region, *Atmos. Res.*, 2017, **187**, 106–127.

82 W. Jia and X. Zhang, The role of the planetary boundary layer parameterization schemes on the meteorological and aerosol pollution simulations: A review, *Atmos. Res.*, 2020, **239**, 104890.

83 G. Mancheno, J. Castro-Molinare and H. Jorquera, Predictive modeling the effect of Local Climate Zones (LCZ) on the urban meteorology in a tropical Andean area, *Model. Earth Syst. Environ.*, 2024, **10**, 6133–6153, DOI: **10.1007/s40808-024-02121-0**.

84 D. C. Carslaw and K. Ropkins, openair—An R Package for Air Quality Data Analysis, *Environ. Model. Softw.*, 2012, **27–28**, 52–61, DOI: **10.1016/j.envsoft.2011.09.008**.

85 J. C. Chang and S. R. Hanna, Air quality model performance evaluation, *Meteorol. Atmos. Phys.*, 2004, **87**(1–3), 167–196, DOI: **10.1007/s00703-003-0070-7**.

86 C. Emery, E. Tai and G. Yarwood, *Enhanced Meteorological Modeling and Performance Evaluation for Two Texas Ozone Episodes*, prepared for the Texas Natural Resource Conservation Commission, 2001.

87 W. Y. Appel, C. Chemel, S. J. Roselle, *et al.*). Examination of the Community Multiscale Air Quality (CMAQ) model performance over the North American and European domains, *Atmos. Environ.*, 2013, **53**, 142–155, DOI: **10.1016/j.atmosenv.2011.11.016**.

88 R. Jat, C. Jena, P. P. Yadav, G. Govardhan, G. Kalita, S. Debnath, P. Gunwani, P. Acharja, P. V. Pawar, P. Sharma, S. H. Kulkarni, A. Kulkarni, A. Kaginalkar, D. M. Chate, R. Kumar, V. K. Soni and S. D. Ghude, Evaluating the sensitivity of fine particulate matter (PM2.5) simulations to chemical mechanism in WRF-Chem over Delhi, *Atmos. Environ.*, 2024, **323**, 120410, DOI: **10.1016/j.atmosenv.2024.120410**.

89 C. Wiedinmyer, S. K. Akagi, R. J. Yokelson, L. K. Emmons, J. A. Al-Saadi, J. J. Orlando and A. J. Soja, The Fire INventory from NCAR (FINN): A high resolution global model to estimate the emissions from open burning, *Geosci. Model Dev.*, 2011, **4**(3), 625–641, DOI: **10.5194/gmd-4-625-2011**.

90 EP Petroecuador, Annual Statistical Report 2018, 2018, **https://www.eppetroecuador.ec/wp-content/uploads/2024/06/INFORME-ESTADISTICO-2018.pdf**.

91 Ministerio del Ambiente del Ecuador, *Informe de Rendición de Cuentas 2018*, Dirección Provincial del Ambiente de Pichincha, Quito, Ecuador, 2019, **https://www.ambiente.gob.ec/wp-content/uploads/downloads/2019/03/Informe_RC_2018_DP_Pichincha.pdf**.

92 L. Dawidowski, J. Gelman Constantin, J. Herrera Murillo, M. Gómez-Marín, T. Nogueira, S. Blanco Jiménez, V. Díaz-Suárez, F. Baraldo Victorica, P. Lichtig, M. Díaz Resquin, M. Vargas-Rojas, J. Murillo-Hernández, J. A. Vergara Correa, M. F. Andrade, D. M. Dos Santos, J. Flores Maldonado, F. Aldape, L. F. Abreu and M. I. Manousakas, Carbonaceous fraction in PM2.5 of six Latin American cities: Seasonal variations, sources and secondary organic

© 2025 The Author(s). Published by the Royal Society of Chemistry

Environ. Sci.: Adv., 2025, **4**, 1310–1332 | **1331**

carbon contribution, *Sci. Total Environ.*, 2024, **948**, 174630, DOI: **10.1016/j.scitotenv.2024.174630**.

93 R. Zalakeviciute, K. Alexandrino, D. Mejia, M. G. Bastidas, N. H. Oleas, D. Gabela, P. N. Chau, S. Bonilla-Bedoya, V. Diaz and Y. Rybarczyk, The effect of national protest in Ecuador on PM pollution, *Sci. Rep.*, 2021, **11**, 17591, **https://www.nature.com/articles/s41598-021-96868-6**.

94 R. Atkinson and J. Arey, Gas-phase tropospheric chemistry of biogenic volatile organic compounds: A review, *Atmos. Environ.*, 2003, **37**(2), 197–219, DOI: **10.1016/S1352-2310(03)00391-1**.

95 A. Guenther, T. Karl, P. Harley, C. Wiedinmyer, P. I. Palmer and C. Geron, The Model of Emissions of Gases and Aerosols from Nature version 2.1 (MEGAN2.1): An extended and updated framework for modeling biogenic emissions, *Geosci. Model Dev.*, 2012, **5**(6), 1471–1492, DOI: **10.5194/gmd-5-1471-2012**.

96 K. C. Wells, D. B. Millet, V. H. Payne, M. J. Deventer, K. H. Bates, J. A. de Gouw, M. Graus, C. Warneke, A. Wisthaler and J. D. Fuentes, Satellite isoprene retrievals constrain emissions and atmospheric oxidation, *Nature*, 2020, **585**(7824), 225–233, DOI: **10.1038/s41586-020-2664-3**.

97 M. Morichetti, S. Madronich, G. Passerini, U. Rizza, E. Mancinelli, S. Virgili and M. Barth, Comparison and evaluation of updates to WRF-Chem (v3.9) biogenic emissions using MEGAN, *Geosci. Model Dev.*, 2022, **15**, 6311–6339, DOI: **10.5194/gmd-15-6311-2022**.

98 H.-J. Lee, H.-Y. Jo, C.-K. Song, Y.-J. Jo, S.-Y. Park and C.-H. Kim, Sensitivity of simulated PM2.5 concentrations over Northeast Asia to different secondary organic aerosol modules during the KORUS-AQ campaign, *Atmosphere*, 2020, **11**(9), 1004, DOI: **10.3390/atmos11091004**.

99 U.S. Environmental Protection Agency (U.S. EPA), *Guidance on the Use of Models and Other Analyses for Demonstrating Attainment of Air Quality Goals for Ozone, PM2.5, and Regional Haze (EPA-454/B-07-002)*, Office of Air Quality Planning and Standards, 2007.